Influence of mesoporous materials containing ZSM-5 on alkylation and cracking reactions

T. Odedairo, R.J. Balasamy, S. Al-Khattaf*

Center of Excellence in Petroleum Refining and Petrochemicals, King Fahd University of Petroleum & Minerals, Dhahran 31261, Saudi Arabia

ARTICLE INFO

ABSTRACT

In order to increase the yield of cymene in alkylation of toluene with isopropanol, ZSM-5 zeolite units were incorporated into a mesostructured material. The catalysts were characterized by X-ray diffraction, TGA, SEM, NH_3 temperature-programmed desorption and FTIR of pyridine adsorption. XRD analysis indicated that a structurally well ordered cubic MCM-48 aluminosilicate was successfully assembled from ZSM-5 zeolite seeds. The ZSM-5/MCM-48 catalyst exhibited significantly improved toluene conversion and yield of cymene product for toluene isopropylation. Catalytic tests show that the ZSM-5/MCM-48 composite material exhibits high catalytic activity compared with the conventional Y-zeolite for catalytic cracking of 1,3,5-triisopropylbenzene (TIPB). The exceptional catalytic performance of ZSM-5/MCM-48 catalyst in cracking and alkylation reaction was attributed to the easier access of active sites provided by the mesopores for both reactant and larger product molecules. The apparent activation energies for the cracking of 1,3,5-TIPB over ZSM-5/MCM-48 catalyst were found to decrease as follows: $E_{C/CM-3 \text{ (tertiary cracking)}} > E_{C/CM-4 \text{ (disproportionation)}} > E_{C/CM-2 \text{ (secondary cracking)}} > E_{C/CM-1 \text{ (primary cracking)}}$.

1. Introduction

The demand for advancement in zeolite science and technology has been persistent over the past 40 years [1]. Refineries need to improve the processing of heavy feedstocks into more valuable environmental friendly lighter products. Microporous molecular sieves such as zeolite Y, ZSM-5 and β which have abundant uniform microporous structures and strong intrinsic acidities, have played important roles in acid catalysis [2]. However, due to their limited pore size range (maximum pore size is typically <1.5 nm), much effort has been devoted to the development of new zeolite-type materials with larger (>1.5 nm) pores [3,4]. The discovery of ordered mesoporous materials, such as M41S, provides the opportunity of overcoming the diffusion limitation for bulky molecules involved in catalytic reactions [5]. However, due to the amorphous nature of their frameworks, M41S-type mesoporous aluminosilicates generally exhibit low stability and acidity compared to zeolites, which limits their potential applications [6,7].

Upgrading the performances of mesoporous and microporous molecular sieves, led to the synthesis of new materials which combine the advantages of mesoporous materials with those of zeolites [8–17]. Kloetstra et al. [8] prepared zeolite faujasite overgrown with a thin layer of mesoporous MCM-41, by successive synthesis of FAU and MCM-41 or by adding FAU crystals to MCM-41 synthesis gel. Karlsson et al. [9] prepared composite materials by simultaneously synthesis of MFI/MCM-41 phases using a two-template approach at optimized template concentrations and reaction temperatures. Prokesova et al. [18] reported the preparation of nanosized micro/mesoporous composite materials consisting of zeolite beta and cubic phase MCM-48. Lately, a composite micro/mesoporous ZSM-5/MCM-48 material was prepared using a simple two step crystallization process [7].

Cymenes, specially the para and the meta isomers, are important starting materials for the production of a range of intermediates and end products, such as cresols, fragrances, pharmaceuticals, herbicides, heat transfer media [19–21]. Alkylation of toluene with isopropyl alcohol produces mainly a mixture of cymene isomers. The most preferred isomer distribution requires low ortho-cymene content, since ortho-cymene is difficult to oxidize and inhibits the oxidation of the other isomers. Wichterlova and Cejka [22,23] investigated the alkylation of toluene with isopropanol in relation to time-on-stream with the large pore zeolites Y, beta, mordenite and ZSM-12 and medium pore MFI silicates with aluminum, iron in the framework. Alkylation of toluene with isopropyl alcohol on molecular sieves possessing different acidity and structure type (Y, mordenite and MFI structure) was studied by Cejka et al. [24]. Toluene isopropylation was reported to be controlled by the desorption/transport of bulky reactants, propyltoluenes, out of the inner void volume of the molecular sieves. Recently, alkylation and transalkylation of alkylbenzenes in cymene production was reported over zeolite catalysts [25]. The maximum cymene yield was noticed over a dual-zeolite based catalyst in toluene

* Corresponding author. Tel.: +966 3 860 1429; fax: +966 3 860 4234.
E-mail address: skhattaf@kfupm.edu.sa (S. Al-Khattaf).

isopropylation. Valtierra et al. [26] studied alkylation of toluene with isopropanol over MCM-41/γ-Al$_2$O$_3$ catalysts, and found that the isopropyl toluene fraction contains more para isomer. Savidha and Pandurangan [27] compared mesoporous materials, large pore zeolites and medium pore zeolites for the catalytic isopropylation of toluene with isopropyl acetate. The activity and selectivity to para-cymene of Zn and Fe substituted Al-MCM-41 catalysts were found to be always higher than those of pure Al-MCM-41 catalysts. Yadav and Purandare [28] reported superior activity and selectivity for p-cymene in the alkylation of toluene with 2-propanol over a novel mesoporous solid acid UDCaT-4.

Fluid catalytic cracking (FCC) continues to remain a novel process for production of diesel fuels and high octane gasoline from low value heavy feedstocks [29]. Feedstocks of FCC units have become heavier in the recent years [30,31]. Since the majority of the active sites of the zeolite are within its pores, the cracking of heavier feedstocks tends to be more diffusion controlled. Therefore, it is of great scientific importance to upgrade the performance of the microporous molecular sieves in cracking of the heavy feedstocks. Effects of steaming changes in physicochemical properties of Y-zeolite on cracking of bulky 1,3,5-triisopropylbenzene was investigated by Bazyari et al. [32]. A linear relationship between the cracking activity and the number of framework Al atoms present in the unit cell of zeolites was observed. Morales-Pacheco et al. [33] studied the correlation between the mean crystallites size and catalytic performance of nanometric FAU (Y) and MFI (ZSM-5) in the cracking of 1,3,5-triisopropylbenzene. Two regimes affecting the FCC catalyst operation was reported by Al-Khattaf et al. [34] during their study on the diffusion and catalytic cracking of 1,3,5-TIPB in FCC catalysts. The catalytic cracking of 1,3,5-triisopropylbenzene was also studied over a novel mesoporous beta catalyst [35]. The mesoporous beta showed high catalytic activity as compared with the convectional microporous beta zeolites. Sun et al. [36] reported sulfated zirconia supported in MCM-41 to be an excellent candidate as a catalyst for catalytic cracking of large molecules.

Formation of micro-mesoporous materials is extremely effective to improve their performance in practical applications. In this work, we report the alkylation of toluene with isopropanol over ZSM-5/MCM-48 composite material and the conventional Y-zeolite. The catalytic properties of the ZSM-5/MCM-48 composite material was also investigated for the catalytic cracking of 1,3,5-triisopropylbenzene, and its catalytic activity compared with the conventional microporous Y-zeolite. There is no report available to our knowledge on the use of a composite micro/mesoporous ZSM-5/MCM-48 material for the alkylation of toluene with isopropanol. Kinetic parameters for the disappearance of toluene via alkylation and disproportionation pathways will be determined using the catalyst activity decay function based on time-on-stream. Also, a simplified kinetic model which describes the dominant steps in the catalytic cracking of 1,3,5-triisopropylbenzene, will be developed.

2. Experimental

2.1. Synthesis of catalytic materials

The composite micro-mesoporous materials were synthesized hydrothermally using gel composition of 1 TEOS:0.12 CTAB:0.5 OH:0.03 Al:118 H$_2$O. Tetraethyl orthosilicate (TEOS, Aldrich) and aluminum isopropoxide (Aldrich) were used as the source of silicon and aluminum, respectively. Tetrapropylammonium hydroxide (TPAOH, 10% in water, Aldrich) and cetyltrimethylammonium bromide (CTAB, Merck) were used as the template and secondary template for the formation of micropores and mesopores, respectively. In a typical synthesis procedure, the precursor zeolite colloidal species was prepared by mixing TPAOH, aluminum isopropoxide and water with 21.24 g tetraethyl orthosilicate (TEOS) under stirring. The mixture was then aged at 100 °C for 2 h. Afterwards, the mixture was cooled at room temperature, before it was added to a surfactant (cetyltrimethylammonium bromide) solution containing sodium hydroxide. The gel was then mixed for additional 2 h at room temperature. The crystallization was carried out under static conditions in 130 ml Teflon-lined autoclaves at 150 °C for 8 h. The resulting as-synthesized solid product was recovered by filtration and dried in air. The template and organic additives were removed by calcination at 550 °C for 6 h with ramp of 3 °C/min. The calcined sodium containing sample was then subjected to three-time repeated ion-exchanged with 0.05 M NH$_4$NO$_3$ solution, followed by calcination at 500 °C for 4 h. The synthesis procedure is generally similar to that used for the preparation of zeolite-seed containing mesoporous aluminosilicates [11–13].

The commercial Y-zeolite having a Si/Al ratio of 3.2 used in this work was obtained from Tosoh Company in the Na form. The zeolite was ion exchanged with NH$_4$NO$_3$ to replace the sodium cation with NH4$^+$. The process of sodium removal was repeated for the pelletized catalyst. Following this, the catalyst was calcined for 2 h at 600 °C.

2.2. Characterization of catalysts

The catalysts were characterized by X-ray power diffraction (XRD), thermogravimetric analysis (TGA), NH$_3$ temperature-programmed desorption (NH$_3$-TPD), FTIR of pyridine adsorption and nitrogen adsorption–desorption to understand the textural and chemical properties of micro-mesoporous material (ZSM-5/MCM-48) and to compare it with the conventional microporous Y-zeolite.

Powder X-ray diffraction (XRD) was recorded on a Mac Science MX18XHF-SRA powder diffractometer with monochromatized Cu Kα radiation (λ = 0.154 nm) at 40 kV and 30 mA. Thermogravimetric analysis (TGA) was performed using a TA Instrument SDT Q 600 TGA analyzer with a heating rate of 10 °C/min under a nitrogen flow.

Concentration of Lewis and BrØnsted acid sites was determined after adsorption of pyridine by FTIR spectroscopy (Nicolet 6700 FTIR). Samples were pressed into self-supporting wafers with a density of 8.0–12 mg/cm^2 and activated in situ at 430 °C overnight. Pyridine adsorption was carried out at 150 °C for 20 min at partial pressure 800–1000 Pa, followed by desorption for 15 min.

The acidic properties of all catalysts were characterized by NH$_3$ temperature-programmed desorption (NH$_3$-TPD). In all the experiments, 50 mg of sample were outgased at 400 °C for 30 min in flowing He and then cooled to 150 °C. At that temperature, NH$_3$ was adsorbed on the sample by injecting pulses of 2 μL/pulse. The injection was repeated until the amount of NH$_3$ detected was the same for the last two injections. After the adsorption of NH$_3$ was saturated, the sample was flushed at 150 °C for 1 h with He to remove excess NH$_3$, and then the temperature was programmed at 30 °C/min up to 1000 °C in flowing helium at 30 mL/min. A thermal conductivity detector was used to monitor the desorbed NH$_3$.

Nitrogen sorption isotherms were performed at liquid nitrogen temperature (-196 °C) on a Quantachrome AUTOSORB-1 (model ASI-CT-8). Prior to the sorption measurements, all samples were degassed at 250 °C for at least 24 h until pressure of 10^{-3} Pa was attained. The surface area was calculated using the Brunauer–Emmett–Teller (BET) method. The total pore volume was determined from the amount of nitrogen adsorbed at P/P_0 = ca. 0.99. The Barrett–Joyner–Halenda (BJN) [37] method and t-plot analysis were used to determine the micropore surface area and pore volume. Scanning electron microscopy (SEM) image was recorded using a JEOL, JSM-5500LV scanning electron microscope.
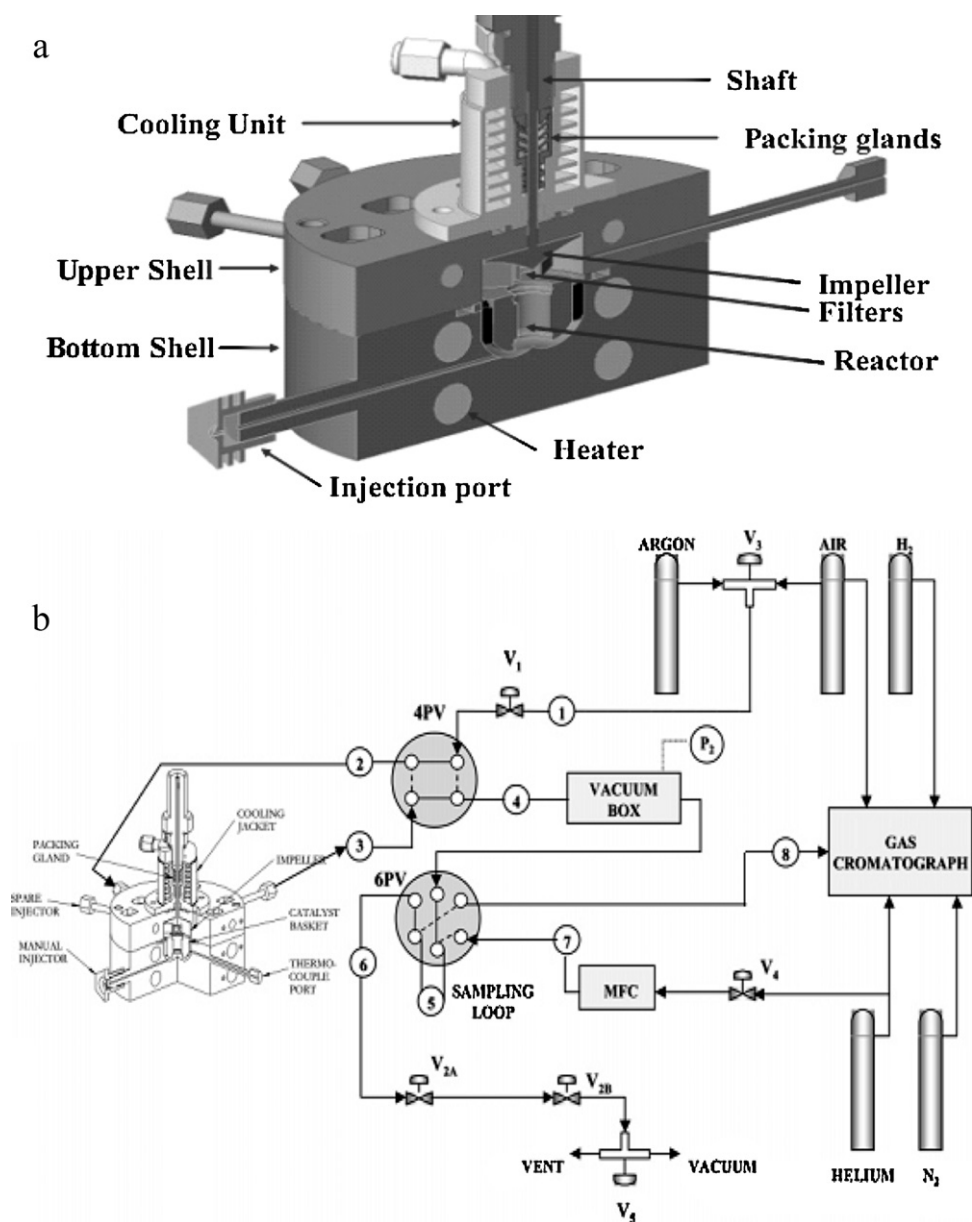
Fig. 1. (a) Schematic diagram of the riser simulator and (b) schematic diagram of the riser simulator experimental set-up.

2.3. Reaction apparatus and procedures

Both alkylation and catalytic cracking reactions were carried out in the riser simulator (see Fig. 1) and were operated under atmospheric pressure. This reactor is novel bench-scale equipment with an internal recycle unit invented by de Lasa [38]. Catalytic experiments were performed at a catalyst/reactant ratio of 3.75 (weight of catalyst = 0.60 g) for different residence times of 5, 10 15 and 20 s and at reaction temperatures of 250, 275, 300, 350 and 400 °C. Analytical grade (99% purity) pure toluene, isopropanol and 1,3,5-triisopropylbenzene were obtained from Sigma–Aldrich. All chemicals were used as received, and no attempt was made to further purify the samples. A four-port valve enables the connection and isolation of the 45 cm³ reactor and the vacuum box, and a six-port valve allows for the collection of a sample of reaction products in a sampling loop. The products were analyzed in an Agilent model 6890N gas chromatograph with a flame ionization detector and a capillary column INNOWAX, 60-m cross-

linked methyl silicone with an internal diameter of 0.32 mm. During the course of the investigation, a number of runs were repeated to check for reproducibility in the experiment results, which were found to be excellent. Typical errors were in the range of ±2%.

The amount of coke deposited on the spent catalysts was determined by a common combustion method. In this method, a carbon analyzer multi EA 2000 (Analytikjena) is used. Oxygen is supplied to the unit directly. The multi EA 2000 with CS Module is a specially developed system to permit simultaneous or separate determination of the total carbon and total sulfur in samples of solids, pastes and liquids by means of high temperature oxidation in a current of oxygen. It is based on special HTC (high temperature ceramics) technology which renders a catalyst superfluous. A small amount of the spent catalyst (0.35 g) is used for the analysis. Further clarification on how the amount of coke deposited on the spent catalysts was determined can be found in another paper of the authors [39,40].
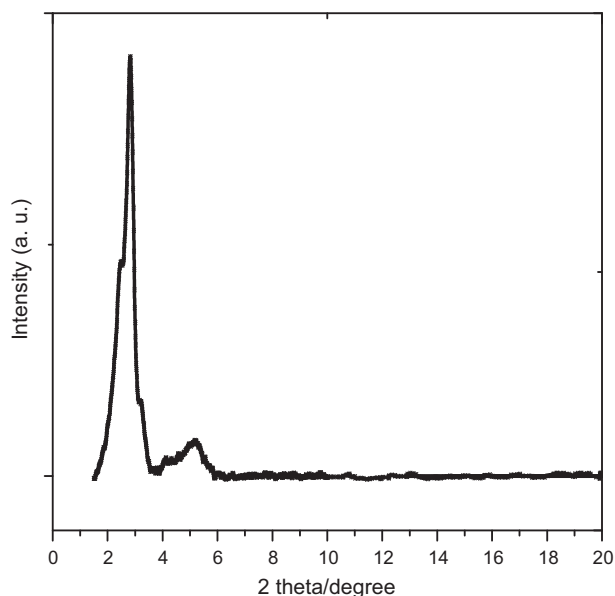
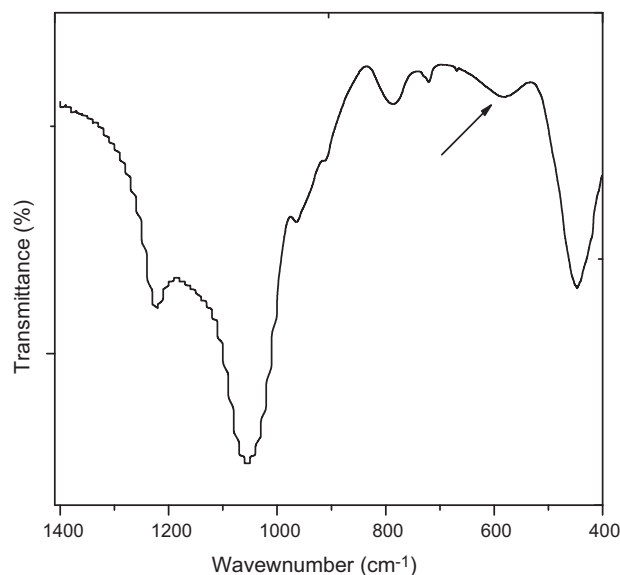**Fig. 2.** Powder XRD pattern of ZSM-5/MCM-48 catalyst.

Fig. 3. IR spectra of calcined ZSM-5/MCM-48 catalyst.

3. Results and discussion

3.1. Characterization of samples used

XRD pattern of the calcined micro-mesoporous ZSM-5/MCM-48 composite material is displayed in Fig. 2. The XRD pattern for the ZSM-5/MCM-48 catalyst had a basal peak (2 1 1) and several other peaks, i.e. (2 2 0), (4 2 0) and (3 3 2), which can be indexed to the cubic (*Ia*3*d*) MCM-48 phase [41,42]. A well ordered cubic MCM-48 aluminosilicate can be said to have been effectively assembled from ZSM-5 zeolite seeds based on the XRD pattern obtained for the ZSM-5/MCM-48 catalyst [7,43]. The wide-angle XRD pattern of ZSM-5/MCM-48 composite material presented in Fig. 2 indicates that the zeolite seeds formed during the crystallization process were used up as structural building units for the construction of the mesoporous materials. Similar observation was reported by Huang et al. [2], when a composite MCM-41/ZSM-5 catalyst showed no diffraction peaks corresponding to long-range ordered ZSM-5 in the high 2θ range.

Infrared spectroscopy is an excellent technique for probing the atomic ordering of zeolite type materials. In order to prove the presence of ZSM-5 structure in the composite material, infrared spectra of the calcined ZSM-5/MCM-48 composite material is presented in Fig. 3. It is evident from Fig. 3 that, a broad but distinct vibration band at 550–600 cm^{-1} is observed in the ZSM-5/MCM-48 composite material. This relatively well developed band at 550–600 cm^{-1} has been assigned to the asymmetric stretching mode of five-membered ring blocks present in the ZSM-5 structure [2,12,13].

Thermogravimetric analysis of as-synthesized sample may be used to probe the presence of zeolite building units in the mesostructured MCM-48 materials [18]. Thermogravimetric analysis (TGA) curve of the as-synthesized composite mesophases is shown in Fig. 4. The ZSM-5/MCM-48 catalyst has a weight loss below 120 °C, which is the result of desorption of water. The organic additives/templates present in the as-synthesized ZSM-5/MCM-48 catalyst were desorbed in three steps. The weight losses noticed in the ZSM-5/MCM-48 catalyst can be attributed to the thermal decomposition of CTAB (150–300 °C) and TPAOH (250–500 °C) [18]. The weight loss for the decomposition of CTAB is ~33%, while the weight loss due to decomposition of TPAOH is ~12%.

Table 1 provides the quantitative evaluation of the FTIR spectra of the catalysts under study. For application of zeolites in acid catalyzed reactions, the concentration of acid sites (BrØnsted and Lewis types) is of utmost importance. The concentration of BrØnsted acid sites and all acid sites of both catalysts under study is presented in Table 1. Fig. 5 presents the FTIR spectra of hydroxyl region of Y-zeolite and the ZSM-5/MCM-48 catalyst after pyridine adsorption and also the spectral area of vibrations of pyridine interaction with different acid sites. Hydroxyl region consists of absorption bands centered around 3742 cm^{-1} (silanol groups), 3670 cm^{-1} (OH groups attached to an extra-framework Al species) and the band at 3610 cm^{-1} (acid bridging OH groups). Adsorption of pyridine resulted in the formation of bands at 1545 cm^{-1} over both catalysts, which is characteristic for pyridine protonated by BrØnsted acid sites and absorption band at 1446 and 1455 cm^{-1} are typical for pyridine interacting with non-acidic OH groups of silica
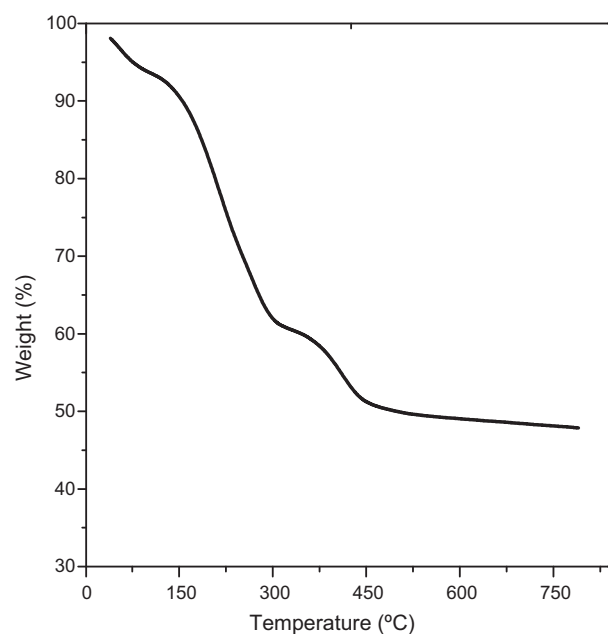

Fig. 4. Thermogravimetric analysis curve of as-synthesized ZSM-5/MCM-48 catalyst.

Table 1
Characterization of catalysts under study.

Catalyst	Acidity (mmol/g)	Surface area (m²/g)	Si/Al ratio	Pore volume (cm³/g)	Pore size (Å)	Lewis sites (mmol/g)	Bronsted sites (mmol/g)
ZSM-5/MCM-48	0.55	1347 (0)	30	0.94 (0)	27.9	0.59	0.10
Al-MCM-48	0.33	808 (0)	21	0.56 (0)	27.7	0.17	0.05
HY	2.99	545 (499)	3.2	0.34 (0.24)		2.39	2.58
ZSM-5	1.15	0 (364)	13.5	0 (0.17)		0.21	0.45

The values in parentheses are the micropore surface area or pore volume. Pore size obtained from the formula, pore size = $4 V_{meso}/S_{meso}$, where V_{meso} is the mesopore volume and S_{meso} is the mesopore surface area.
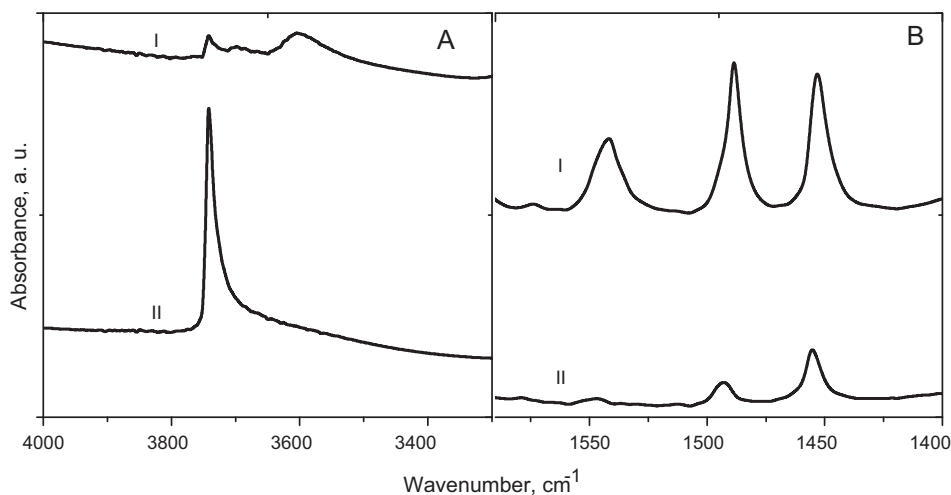

Fig. 5. Infrared spectra of hydroxyl region after pyridine desorption (A) and area of pyridine interacting with Bronsted and Lewis acid sites (B), Y-zeolite (I) and ZSM-5/MCM-48 (II).

or alumina and with typical adsorbed Lewis acid sites, respectively. ZSM-5/MCM-48 catalyst possesses 0.10 mmol/g of BrØnsted sites (14%) and 0.59 mmol/g of Lewis acid sites (86%).

The surface texture of the ZSM-5/MCM-48 composite material was characterized by means of N_2 adsorption–desorption (BET) isotherms as shown in Fig. 6 and the corresponding textural properties are summarized in Table 1. The ZSM-5/MCM-48 material exhibited nitrogen sorption isotherms with a well-defined capillary condensation step in the partial pressure (P/P_0) range 0.2–0.4. This indicates that the sample possess good mesostructural order-

ing [42]. The ZSM-5/MCM-48 material exhibited a BET surface area of 1347 m²/g, pore volume of 0.94 cm³/g and an average pore diameter around 2.4 nm. Acidic and textural properties of catalysts under study are summarized in Table 1. It is obvious that the concentration of acid sites in the commercial Y-zeolite catalyst (2.99 mmol/g) is much higher than the concentration of acid sites noticed in the ZSM-5/MCM-48 catalyst (0.55 mmol/g).
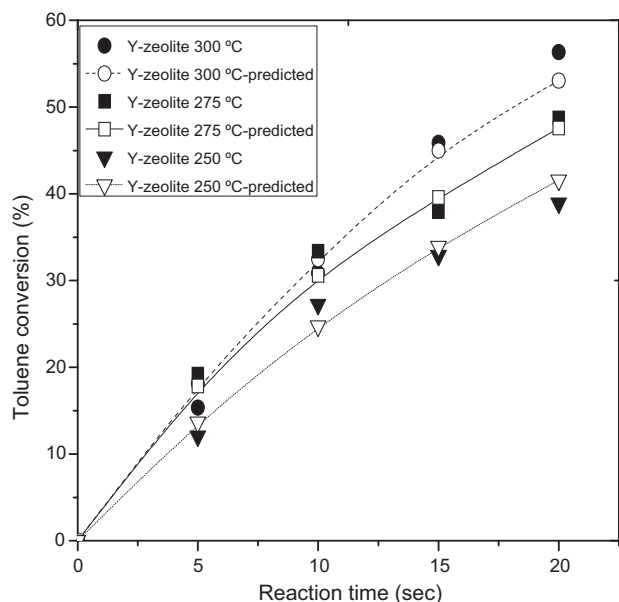
The particle morphology of the ZSM-5/MCM-48 catalyst was studied using scanning electron microscopy. Fig. 7 shows typical SEM image of ZSM-5/MCM-48 catalyst, with aggregated sphere
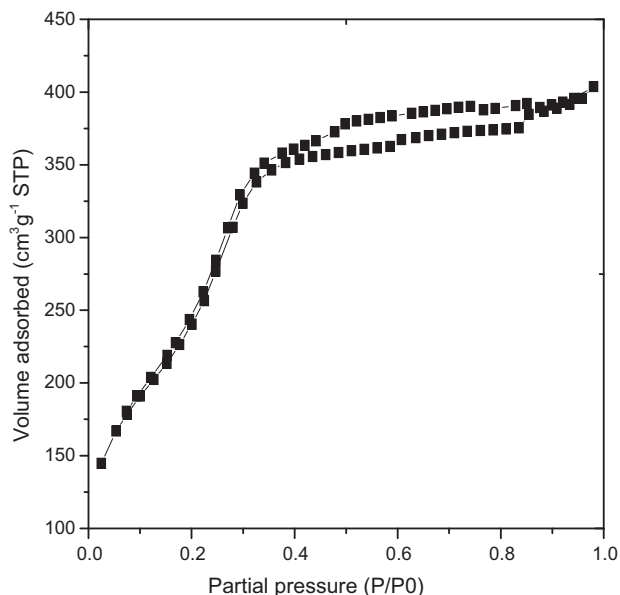
Fig. 6. N_2 adsorption–desorption isotherm of ZSM-5/MCM-48 catalyst.
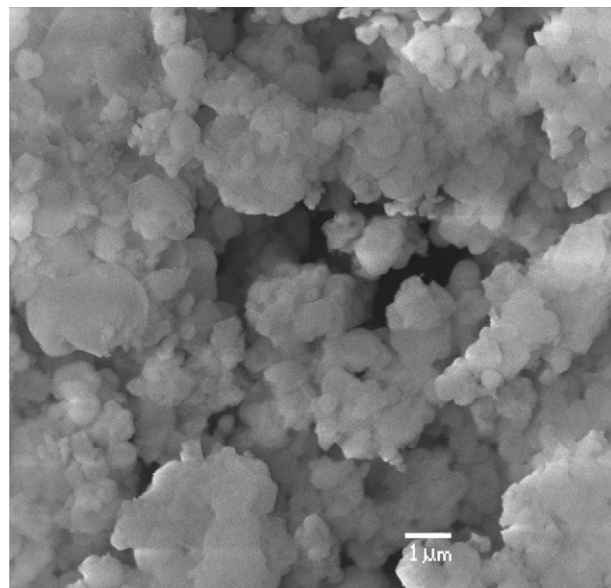
Fig. 7. Scanning electron microscopy (SEM) image of ZSM-5/MCM-48 catalyst.

Fig. 8. Variation of toluene conversion with reaction time achieved over Y-zeolite catalyst in the alkylation reaction of toluene with isopropanol at 250 (▼), 275 (■) and 300 °C (●) for catalyst/feed = 3.75.

shaped particles. The core shell morphology reported for similar cubic mesoporous aluminosilicates was not noticed in the ZSM-5/MCM-48 catalyst [44].

3.2. Alkylation of toluene with isopropanol

The alkylation reaction was carried out at 250, 275 and 300 °C over both Y and ZSM-5/MCM-48 catalyst for residence times of 5, 10, 15 and 20 s with constant toluene to isopropanol molar ratio of 1:1. Mixture of cymenes are the major products produced in the alkylation reaction of toluene with isopropanol, while benzene, xylenes and ethylbenzene are also produced in significant amount, indicating partial toluene disproportionation. Table 2 present conversions and complete product distribution for the alkylation of
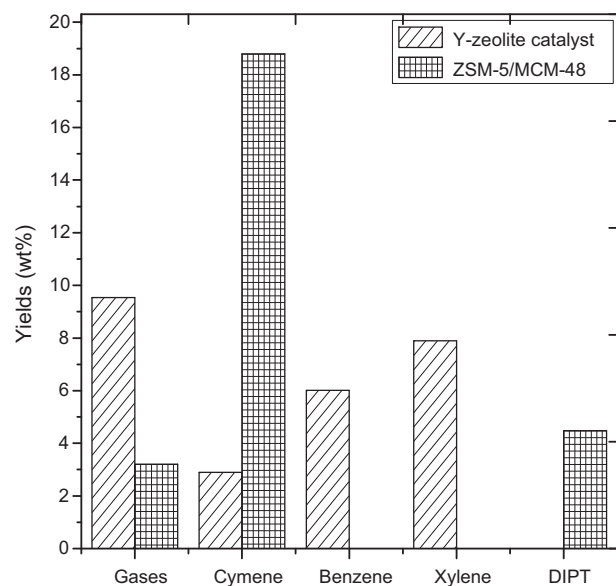
Fig. 9. Product distribution over Y-zeolite catalyst and ZSM-5/MCM-48 catalyst (toluene conversion = ~27%, reaction temperature = 250 and 275 °C, toluene:isopropanol = 1, catalyst/feed = ~3.8).

toluene with isopropanol over ZSM-5/MCM-48 catalyst. A scheme representing an overview of the isopropylation of toluene with isopropanol can be found in another paper of the authors [25].

3.2.1. Effect of reaction temperature on the conversion of toluene and product distribution

Toluene conversions of approximately 24.5, 26.5 and 23.7% were achieved at 250, 275 and 300 °C, respectively, for a residence time of 20 s over the ZSM-5/MCM-48 catalyst, as presented in Table 2. The conversion of toluene increased with contact time, for all the temperature studied. The maximum toluene conversion ~26.5% was observed over ZSM-5/MCM-48 catalyst at 275 °C, for a reaction time of 20 s. The major product of the alkylation reaction of toluene with isopropanol over ZSM-5/MCM-48 catalyst is cymenes. Presence of benzene and xylenes were also noticed in the reaction products at 300 °C over the ZSM-5/MCM-48 catalyst, indicating partial disproportionation of toluene. Gaseous products were among the reaction products noticed in the alkylation reaction over ZSM-5/MCM-48 catalyst for all temperatures studied, indicating that dealkylation or pairing reactions are occurring at these temperatures. Dehydration of isopropanol may also account for the significant amount of gaseous products noticed in the alkylation reaction, as illustrated in Scheme 1. The reaction is initiated when a surface proton attacks isopropanol resulting in the formation of surface isopropyl cation and water. The carbenium ion (dimethyl carbenium ion) which is the key intermediate follows two main reaction pathways. The isopropyl cation either attacks toluene ring carbon atom at the ortho, meta, or para position atom to form protonated cymene or returns a proton to surface, to produce propylene. A maximum cymene yield of ~18.8% was noticed at 275 °C for a reaction time of 20 s. The diisopropyltoluenes (DIPTs) yield decreased with increasing temperature. About 5.6, 4.5 and 2.7% yield of DIPT was observed at 250, 275 and 300 °C, respectively. Reduction in the yield of diisopropyltoluenes with increasing temperature might be due to the pronounced dealkylation or disproportionation of toluene occurring at these temperatures.

Alkylation reaction of toluene with isopropanol was also studied over the conventional microporous Y-zeolite. The conversion of toluene over Y-zeolite increased with increasing reaction temperature and contact time. A maximum toluene conversion of ~56.3% was obtained at 300 °C for a reaction time of 20 s, as shown in Fig. 8. The major products in the alkylation of toluene with isopropanol over the catalyst based Y-zeolite are benzene and xylenes. Significant amounts of cymenes were also noticed at all temperature studied over the conventional microporous Y-zeolite. Cymene yield of approximately 4.1, 2.9 and 1.4% were achieved at 250, 275 and 300 °C, respectively, for a reaction time of 20 s. The yield of the cymene was noticed to decrease with increasing temperature, while the yield of both benzene and xylenes over the Y-zeolite was observed to increase with increasing temperature. The maximum yield of ~10.7% and ~11.7% of benzene and xylenes, respectively, was observed at 300 °C, for a reaction time of 20 s. The trend of the reaction products with increasing temperature indicates that disproportionation of toluene was noticed to be the major reaction occurring at higher temperatures, while the alkylation reaction of toluene with isopropanol was observed to dominate at lower temperature over the conventional microporous Y-zeolite. Absence of diisopropyltoluenes in the reaction products reveals that no secondary alkylation reaction was occurring at all temperatures studied over Y-zeolite catalyst. The amount of gaseous products (31.3%) obtained at 300 °C, reveals the pronounced dealkylation reactions occurring over Y-zeolite catalyst. Yadav and Purandare [28] reported that the alkylation of toluene with isopropanol involves a complex reaction mechanism in that there is dehydration of isopropanol leading to propylene. The possibilities of the propylene produced to undergo oligomerization

Table 2
Product distribution (wt%) at various reaction conditions for alkylation of toluene with isopropanol over ZSM-5/MCM-48 catalyst.

Temp (°C)	Time (s)	Toluene conv. (%)	Gases	Benzene	Xylene	m-Cym	p-Cym	o-Cym	Total Cymene	DIPT's
250										
	5	7.11	–	–	–	2.28	2.16	0.94	5.38	1.73
	10	15.13	0.96	–	–	4.50	4.12	1.79	10.41	3.76
	15	21.03	2.24	–	–	6.12	5.47	2.28	13.87	4.92
	20	24.53	3.18	–	–	7.24	6.16	2.39	15.79	5.56
275										
	5	8.63	0.47	–	–	2.93	2.49	0.95	6.37	1.79
	10	17.11	2.09	–	–	5.23	4.39	1.71	11.33	3.69
	15	22.13	2.98	–	–	7.44	5.73	2.00	15.17	3.98
	20	26.49	3.21	–	–	9.63	6.92	2.25	18.80	4.48
300										
	5	9.61	0.97	–	–	4.13	2.63	0.78	7.54	1.10
	10	16.26	1.77	–	0.01	6.65	4.41	1.36	12.42	2.06
	15	21.52	2.54	–	0.05	9.05	5.83	1.74	16.62	2.31
	20	23.65	3.01	0.05	0.06	9.91	6.05	1.72	17.68	2.65

T = 250–300 °C, and toluene to isopropanol molar ratio 1 and catalyst/feed = 3.8.

depend on the type of catalyst, its acidity and pore size distribution [45,46].

### 3.2.2. Comparison of catalysts in the isopropylation of toluene

The comparison of the product distribution during the alkylation of toluene with isopropanol over Y-zeolite catalyst and the ZSM-5/MCM-48 catalyst is presented in Fig. 9. Over both catalysts, the compositions of the products in the alkylation reaction were compared at similar toluene conversion of ~27%. The results showed that cymene has the highest yield over ZSM-5/MCM-48 catalyst, while the catalyst based on Y-zeolite produced more of gaseous products, mainly propylene. Considerable amounts of benzene (~6%) and xylenes (~7.9%) were found in the alkylation of toluene with isopropanol over the catalyst based on Y-zeolite, as compared with the negligible amount noticed over ZSM-5/MCM-48 catalyst. This result indicates that disproportionation of toluene is one of the major reaction occurring over the catalyst based on Y-zeolite. Fig. 9 shows that the secondary alkylation reaction which involves the alkylation of cymene with isopropanol to produce diisopropyltoluenes is occurring to a great extent over ZSM-5/MCM-48 catalyst. However, little or no secondary alkylation reaction was observed to occur over Y-zeolite catalyst, for all temperature studied, due to absence of diisopropyltoluenes in the reaction products. The effect of toluene conversion on cymene

selectivity at 300 °C over ZSM-5/MCM-48 catalyst and the Y-zeolite catalyst under study is shown in Fig. 10. Cymene selectivity over ZSM-5/MCM-48 catalyst and Y-catalyst shows a low dependence on toluene conversion.

In order to confirm the superior activity of the micro-mesoporous ZSM-5/MCM-48 in the alkylation of toluene with isopropanol in cymene production, alkylation reaction over a pure microporous ZSM-5 and a pure mesoporous Al-MCM-48 was also investigated at 275, 250 and 225 °C. The microporous ZSM-5 has a total acidity of 1.15 mmol/g, with a surface area of ~364 m^2/g, while the pure Al-MCM-48 has an acidity of 0.33 mmol/g and a surface area of 808 m^2/g. The conversions of toluene in the alkylation of toluene with isopropanol over the catalyst based ZSM-5 and the mesoporous Al-MCM-48, were found to be lower than the toluene conversions observed over micro-mesoporous ZSM-5/MCM-48 catalyst. Over the catalyst based on ZSM-5, toluene conversions of approximately 3.7 and 1.5% were achieved at 275 and 250 °C, respectively, for a residence time of 20 s. The maximum cymene yield of ~2.4% was noticed in the alkylation reaction over ZSM-5 based catalyst at 275 °C, for a reaction time of 20 s. Partial disproportionation of toluene was observed to occur over the catalyst based on ZSM-5, due to the traces of benzene and xylenes noticed in the reaction products.
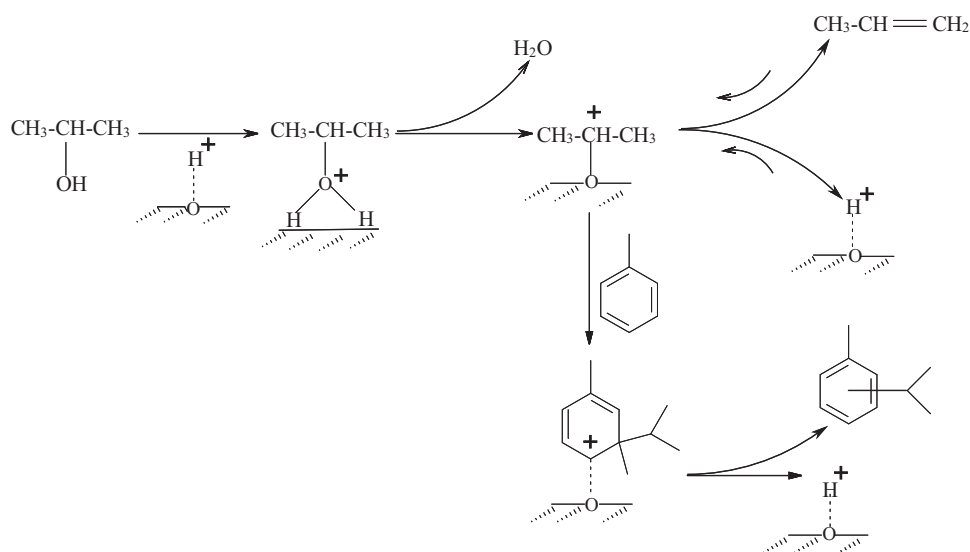
Scheme 1. A possible mechanism for the alkylation of toluene with isopropanol.
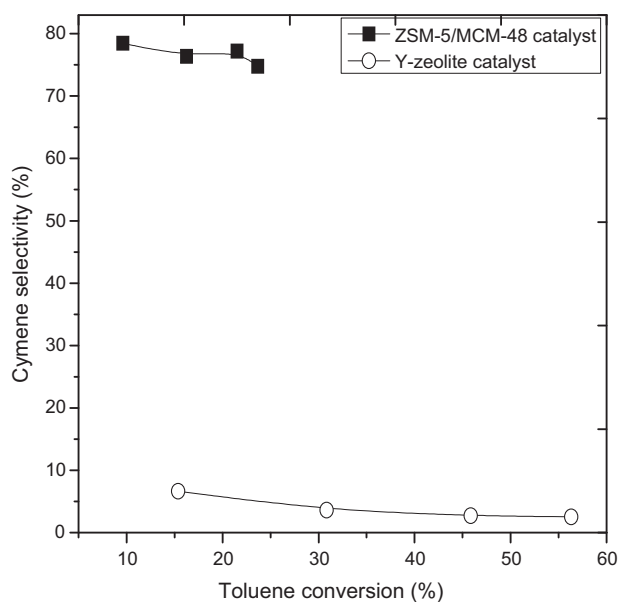
Fig. 10. Effect of toluene conversion on cymene selectivity in alkylation of toluene with isopropanol over ZSM-5/MCM-48 (■) and Y-zeolite catalyst (○) (catalyst/feed = 3.8, reaction temperature = 300 °C).

In the alkylation of toluene with isopropanol over the pure Al-MCM-48, cymenes, diisopropyltoluenes and gaseous hydrocarbon were observed as the major products, while negligible amount of benzene and xylenes were also detected in the reaction products. Toluene conversions of approximately 16.5 and 12% were achieved at 275 °C, at a reaction time of 20 and 15 s respectively. A maximum cymene yield of ~10.5% was noticed at 275 °C for a reaction time of 20 s, which corresponds to a selectivity of ~63.6%.

3.3. Catalytic activity for 1,3,5-triisopropylbenzene cracking

The catalytic cracking performance of the ZSM-5/MCM-48 composite material and the conventional microporous Y-zeolite were tested in a fluidized-bed reactor for catalytic cracking of 1,3,5-triisopropylbenzene at 300, 350 and 400 °C, for reaction time of 5, 10, 15 and 20 s. Regarding the catalytic cracking of 1,3,5-triisopropylbenzene, it is established that the cleavage of the propyl group from the benzene ring is the main reaction pathway with the benzene ring remaining unaltered [47]. Al-Khattaf et al. [34,48] reported that the catalytic cracking of 1,3,5-triisopropylbenzene is a reaction network with three prevailing in series reactions. The authors reported that 1,3,5-triisopropylbenzene dealkylate to 1,3-diisopropylbenzene (1,3-DIPB) and propylene, while the 1,3-DIPB produced further undergoes dealkylation to cumene and propylene. Production of benzene and propylene from the dealkylation of cumene represent the third step of the reaction network proposed. While the above mentioned steps appear as the dominant ones, there are other reactions such as disproportionation, isomerization and condensation that may affect gas phase product distribution and coke formation [47,49]. Tsai et al. [49] reported that the extent of these steps may depend on both temperature and catalyst properties. The catalytic cracking of 1,3,5-TIPB is accompanied by several other reactions as summarized in Fig. 11.

3.3.1. Catalytic cracking of 1,3,5-triisopropylbenzene over ZSM-5/MCM-48 catalyst

The main products obtained from the catalytic cracking of 1,3,5-triisopropylbenzene over ZSM-5/MCM-48 catalyst were benzene, cumene, diisopropylbenzenes and propylene (Table 3). Small amounts of toluene, ethylbenzene and trimethylbenzenes

were also noticed from the reaction products. These compounds (ethylbenzene, xylenes and toluene) are the product of the cracking of the propyl group attached to the benzene ring [50]. A maximum 1,3,5-triisopropylbenzene conversion of ~80.8% was obtained at 400 °C for reaction time of 20 s. The conversion of 1,3,5-triisopropylbenzene was observed to increase with reaction temperature and time. The distribution of 1,3,5-triisopropylbenzene cracking products confirms the domination of the three-step series reactions suggested by Mahgoub and Al-Khattaf [51]. The yield of cumene and benzene increased with reaction time and temperature, up to ~21.6% and ~4.6%, respectively, at 400 °C, for a reaction time of 20 s. An optimum yield of ~25.7% of diisopropylbenzenes was noticed at 350 °C for a reaction time of 20 s. As temperature was further increased to 400 °C, a slight decrease in diisopropylbenzenes yield was noticed to a value of ~18.5%. Meta- and para-diisopropylbenzenes were detected in considerable amount over ZSM-5/MCM-48 catalyst, while only traces of ortho-diisopropylbenzene were noticed in the reaction products. The significant amount of diisopropylbenzenes noticed in the reaction products, indicates that no diffusion limitation was encountered by 1,3,5-triisopropylbenzene molecules, since the production of 1,3-diisopropylbenzene is accompanied by penetration of its precursor (1,3,5-triisopropylbenzene) into the pores of the catalyst and departure of the product from the catalyst surface by diffusing out of the pores.

3.3.2. Catalytic cracking of 1,3,5-triisopropylbenzene over Y-zeolite catalyst

Table 4 shows that propylene, benzene, cumene and toluene were the major products obtained in the catalytic cracking of 1,3,5-triisopropylbenzene over the microporous Y-zeolite catalyst. Traces of diisopropylbenzenes, ethylbenzene, trimethylbenzenes, and xylenes were also detected in the reaction products. 1,3,5-Triisopropylbenzene conversion was found to increase with reaction time for all temperatures studied, reaching maximum of 72.7% at 400 °C. Traces of diisopropylbenzenes noticed in the catalytic cracking of 1,3,5-triisopropylbenzene was found to decrease with increasing temperature. The low yield of diisopropylbenzene may be as a result of 1,3,5-triisopropylbenzene pre-cracking at the surface and/or near surface acid sites of Y-zeolite, leading to some products diffusing into openings and further cracking to lighter products. Bazyari et al. [32] reported that 1,3,5-triisopropylbenzene with the critical diameter of 9.5 Å can diffuse seldom into the highly crystalline Y zeolite structure where most of the acid sites are located. Also, possibility of 1,3,5-triisopropylbenzene dealkylating on weak surface acid sites has been reported by several researchers [52–54]. The yield of benzene was found to increase with both temperature and time, up to a maximum of ~18.7% at 400 °C for a reaction time of 20 s. The pre-cracking taking place at the surface of the Y-zeolite catalyst is also evident by the yield of benzene observed in the reaction products, at all reaction temperatures studied. Cumene selectivity decreased steadily with increase in temperature over Y-zeolite catalyst to minimum of ~3.3% at 400 °C for a reaction time of 20 s. It is evident from Table 4 that as temperature was increased from 300 to 400 °C; more benzene was formed due to cumene cracking, leading to a decrease in the selectivity of cumene at higher temperature.

3.3.3. Comparison of catalysts in the catalytic cracking of 1,3,5-triisopropylbenzene

Fig. 12 provides time-on-steam dependence of 1,3,5-triisopropylbenzene conversion at 400 °C over Y-zeolite catalyst and the ZSM-5/MCM-48 catalyst. It is evident from this figure that, over both catalysts studied, toluene conversion increases as expected with increase in reaction time. The increasing trend of 1,3,5-triisopropylbenzene conversion with reaction time can

be attributed to longer residence time, which results in more contacts of the 1,3,5-triisopropylbenzene molecules and initial products with active sites, resulting in more cracking. The conversion of 1,3,5-triisopropylbenzene was found to be higher over ZSM-5/MCM-48 catalyst as compared with its conversion observed over Y-zeolite catalyst, at most temperatures studied. Although, Y-zeolite catalyst has higher acidity as compared with the acidity of ZSM-5/MCM-48 catalyst, it is widely accepted that catalyst acidity is not the only factor determining conversion and products selectivity and access to catalytically active sites often plays a
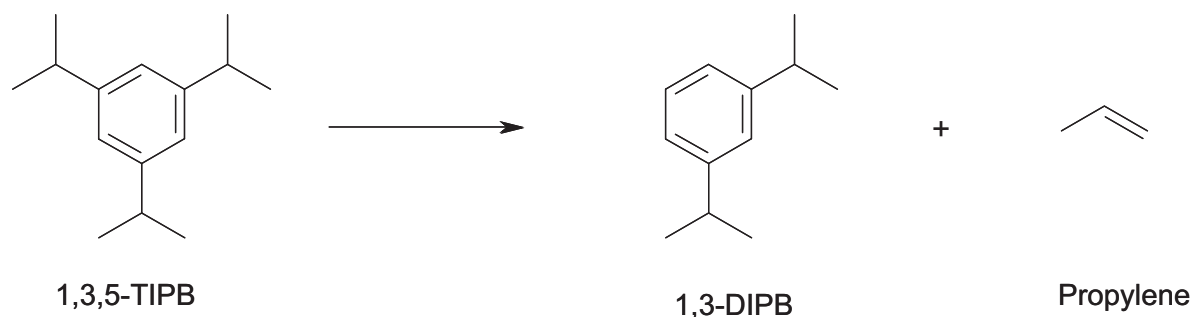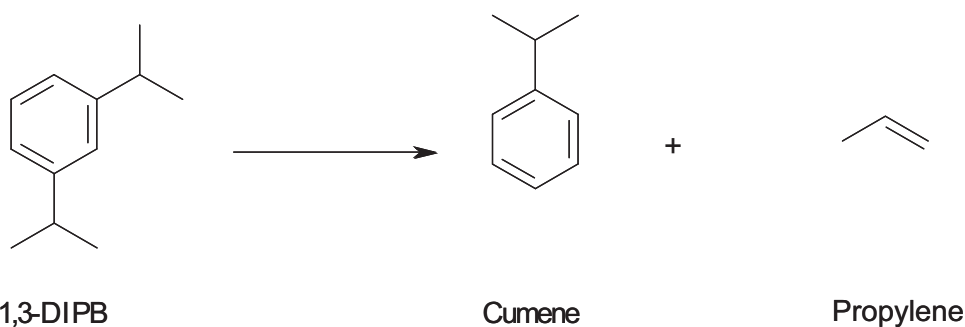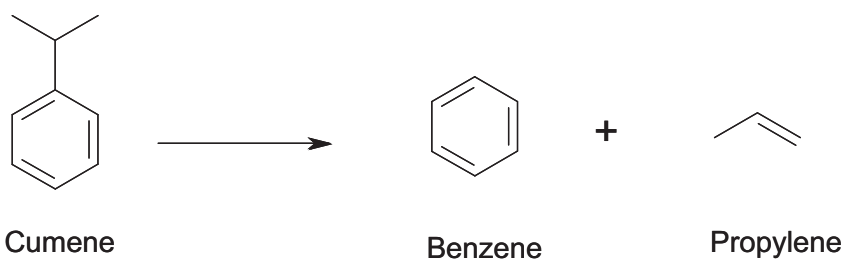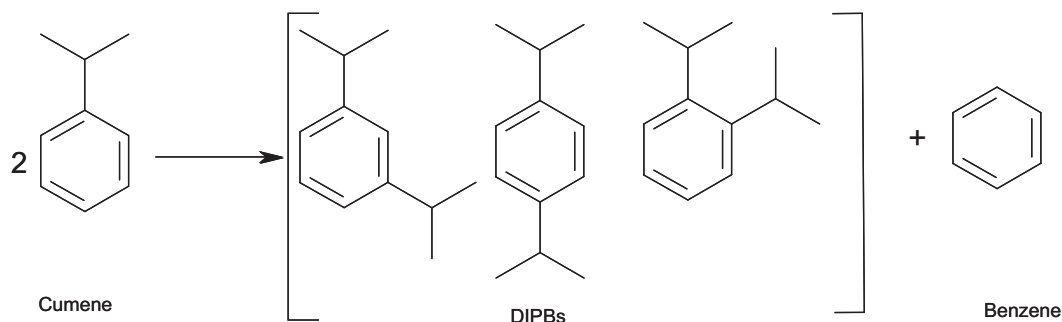
Fig. 11. Reactions occurring during catalytic cracking of 1,3,5-triisopropylbenzene.

Transalkylation of Cumene and 1,3-DIPB

Cumene   1,3-DIPB   1,3,5-TIPB   Benzene

Transalkylation of Cumene and 1,4-DIPB

Cumene   1,4-DIPB   1,2,4-TIPB   Benzene
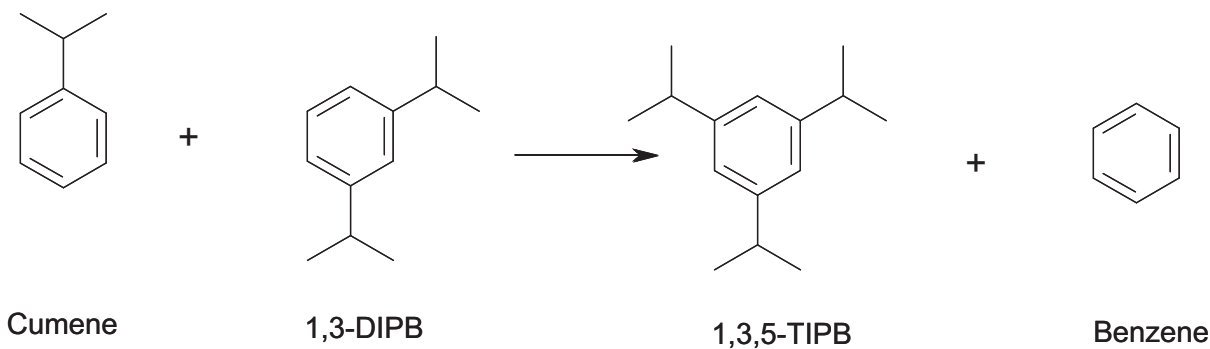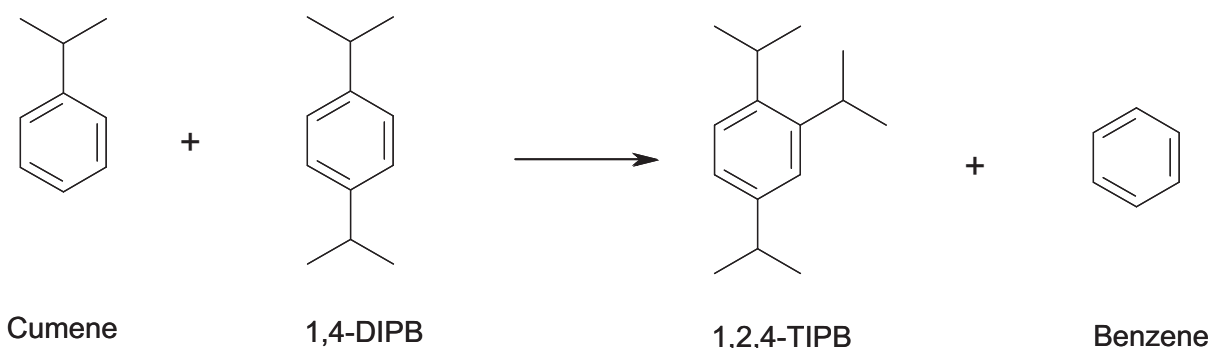
Fig. 11. (Continued).

crucial role in some diffusion-controlled reactions [55]. Also, Fig. 12 shows an increase in 1,3,5-triisopropylbenzene conversion with time-on-stream, which is related to the desorption and transport of products being the rate determining step of the reaction. The presence of mesopores in ZSM-5/MCM-48 catalyst led to a higher conversion compared with the catalyst based on Y-zeolite. It can be proposed that transport of products from the channel system could be more important than their desorption in the catalytic cracking of 1,3,5-triisopropylbenzene over these catalysts. The amount of gaseous products produced in the catalytic cracking of 1,3,5-triisopropylbenzene over both catalysts under study was observed to increase with increasing temperature and time. It

is well known that gases are produced during cracking reaction and that the rate of cracking reaction increases with increasing reaction temperature [56–58].

The comparison of product distribution during the catalytic cracking of 1,3,5-triisopropylbenzene over Y-zeolite catalyst and the ZSM-5/MCM-48 catalyst is presented in Fig. 13. The composition of the products was compared at a constant 1,3,5-triisopropylbenzene conversion of ~47%. Over both catalysts, gaseous products (mainly propylene) were noticed as the major product in the catalytic cracking (Fig. 13). Significant amount of diisopropylbenzenes (~17.8%) was observed in catalytic cracking of 1,3,5-triisopropylbenzene over ZSM-5/MCM-48 catalyst

Table 3
Product distribution (wt%) at various reaction conditions for catalytic cracking of 1,3,5-triisopropylbenzene over ZSM-5/MCM-48 catalyst.

Temp (°C)	Time (s)	1,3,5-TIPB conv. (%)	Gases	Toluene	Benzene	EB	Cumene	TMB's	m-DIPB	p-DIPB	o-DIPB	Total DIPBs
300												
	5	32.47	14.34	–	0.34	0.26	5.58	0.53	8.76	2.51	0.15	11.42
	10	46.29	19.33	–	0.36	0.31	7.68	0.80	12.90	3.67	0.24	17.81
	15	48.57	19.58	–	0.38	0.33	7.70	0.88	15.10	4.33	0.27	19.70
	20	58.16	22.80	–	0.82	0.52	10.94	1.08	16.89	4.81	0.30	22.00
350												
	5	31.82	13.78	–	0.46	0.34	6.95	0.46	7.78	1.94	0.11	9.83
	10	47.07	16.41	–	0.59	0.45	9.91	0.87	14.90	3.73	0.21	18.84
	15	59.11	21.71	–	0.68	0.47	10.94	1.10	18.93	5.01	0.27	24.21
	20	70.55	23.61	0.19	1.49	0.71	15.94	1.40	20.37	5.05	0.31	25.73
400												
	5	39.29	16.68	0.10	1.97	0.49	8.93	0.54	8.57	1.90	0.11	10.58
	10	63.47	21.18	0.15	3.19	0.83	15.24	1.02	12.87	2.92	0.19	15.98
	15	74.34	25.30	0.21	3.61	1.03	18.51	1.33	14.60	3.49	0.25	18.34
	20	80.81	28.62	0.28	4.55	1.25	21.60	1.43	14.70	3.52	0.27	18.49

TIPB – triisopropylbenzene, EB – ethylbenzene, TMB's – trimethylbenzenes, DIPB – diisopropylbenzene, temperature = 300–400 °C and catalyst/feed = 3.8.

Table 4
Product distribution (wt%) at various reaction conditions for catalytic cracking of 1,3,5-triisopropylbenzene over Y-zeolite catalyst.

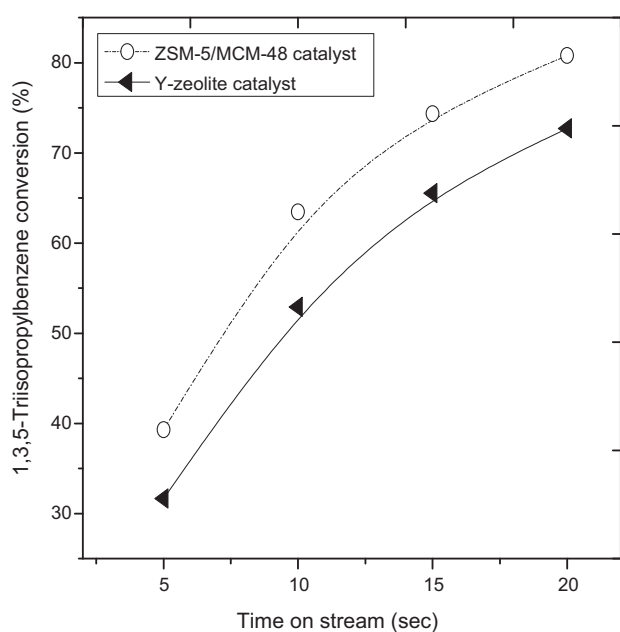| Temp (°C)	Time (s)	1,3,5-TIPB conv. (%)	Gases	Toluene	Benzene	EB	XY	CUM	TMB's	m-DIPB	p-DIPB	o-DIPB	T. DIPBs
300													
	5	30.49	15.60	2.70	8.86	1.15	0.14	1.59	–	0.45	–	–	0.45
	10	40.27	22.51	3.39	11.52	2.28	0.66	3.57	–	0.99	0.10	–	1.09
	15	47.12	22.54	3.88	12.45	2.45	0.79	3.72	–	1.08	0.21	–	1.29
	20	53.23	25.31	4.39	13.38	2.71	0.93	4.99	0.06	1.23	0.23	–	1.46
350													
	5	24.39	17.27	1.07	4.72	0.41	0.09	0.63	–	0.20	–	–	0.20
	10	50.11	29.68	3.69	11.65	1.24	0.74	2.21	0.14	0.60	0.16	–	0.76
	15	64.17	37.69	4.96	14.69	1.63	1.09	3.07	0.18	0.66	0.20	–	0.86
	20	70.06	40.63	5.58	16.05	1.83	1.26	3.50	0.20	0.69	0.22	–	0.91
400													
	5	31.64	21.05	2.17	7.06	0.54	0.39	0.35	–	0.08	–	–	0.08
	10	52.89	31.67	4.34	13.09	1.20	0.91	1.41	0.06	0.21	–	–	0.21
	15	65.54	38.03	5.61	16.28	1.60	1.25	2.38	0.09	0.23	0.07	–	0.30
	20	72.71	40.71	6.81	18.65	1.75	1.67	2.39	0.40	0.25	0.08	–	0.33

XY – xylene, CUM – cumene, TIPB – triisopropylbenzene, EB – ethylbenzene, TMB's – trimethylbenzenes, DIPB – diisopropylbenzene, temperature = 300–400 °C and catalyst/feed = 3.8.

as compared with ∼1.3% noticed over Y-zeolite catalyst. Similarly, ∼7.7% cumene yield was noticed in the cracking reaction over ZSM-5/MCM-48 catalyst, as compared with ∼3.7% observed over Y-zeolite catalyst. On the other hand, significant amount of benzene ('12.5%) was noticed in the catalytic cracking of 1,3,5-triisopropylbenzene over Y-zeolite catalyst as compared with only 0.4% benzene observed over ZSM-5/MCM-48 catalyst. Pre-cracking of 1,3,5-triisopropylbenzene taking place at the surface of the Y-zeolite catalyst, might be responsible for the low yield of diisopropylbenzenes noticed over the catalyst. The production of larger amount of benzene noticed over Y-zeolite catalyst as compared to the yield of benzene observed over ZSM-5/MCM-48 catalyst, can be attributed to the pre-cracking of 1,3,5-triisopropylbenzene and/or difference in acidity of Y-zeolite catalyst and ZSM-5/MCM-48 catalyst. The concentration of acidic site in Y-zeolite catalyst (2.99 mmol/g) is much higher than for ZSM-5/MCM-48 catalyst (0.55 mmol/g). The acidity as well as the pore size of both catalysts play a significant role in the catalytic cracking of 1,3,5-triisopropylbenzene.
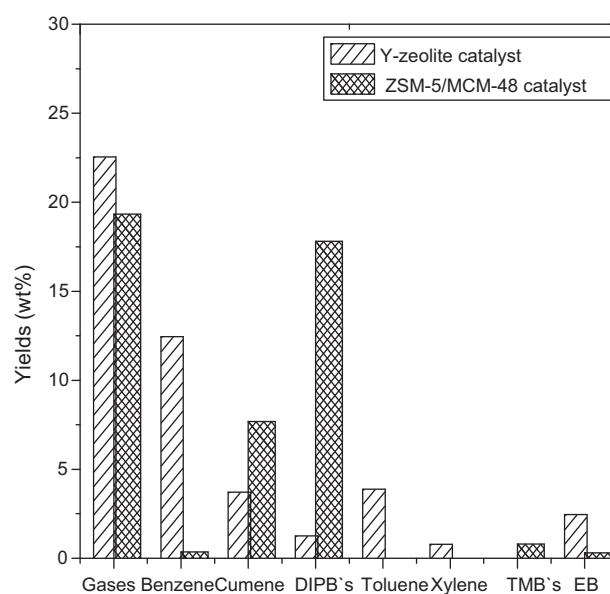
The effect of 1,3,5-TIPB conversion on benzene and cumene selectivity at 400 °C over ZSM-5/MCM-48 catalyst and Y-zeolite catalyst is given in Fig. 14. Benzene selectivity over Y-zeolite catalyst shows a moderate dependence on 1,3,5-TIPB conversion and was observed to increase as 1,3,5-TIPB conversion increases. Benzene selectivity over ZSM-5/MCM-48 catalyst on the other hand, shows a low dependence on 1,3,5-TIPB conversion. Cumene selectivity over both Y-zeolite and ZSM-5/MCM-48 catalyst shows a moderate dependence on 1,3,5-TIPB conversion and was noticed to increase with increasing 1,3,5-TIPB conversion.

3.4. Coke content measurement

Coke was measured at different reaction conditions over Y-zeolite and the ZSM-5/MCM-48 catalyst. Table 5 reveals the amount of coke deposition on the spent catalysts after the reaction. Coke deposited over Y-zeolite catalyst in the alkylation of toluene with isopropanol was found to be higher than the coke noticed over ZSM-5/MCM-48 catalyst. In the alkylation reaction over Y-zeolite catalyst, ∼4.5 wt% of coke was noticed at 300 °C for a reaction time

Fig. 12. Time-on-stream dependence of 1,3,5-triisopropylbenzene conversion over ZSM-5/MCM-48 (○) and Y-zeolite catalyst (◄) at 400 °C for catalyst/feed = 3.8.
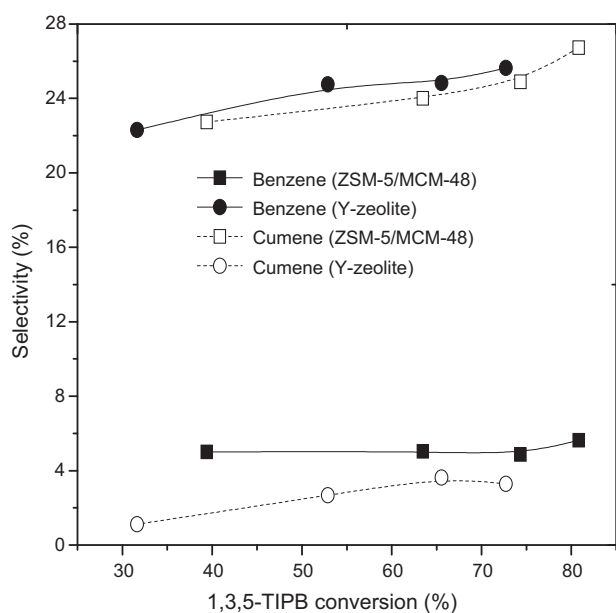

Fig. 13. Product distribution in the catalytic cracking of 1,3,5-triisopropylbenzene over Y-zeolite catalyst and the ZSM-5/MCM-48 catalyst (1,3,5-triisopropylbenzene conversion = ∼47%, reaction temperature = 300 °C, catalyst/feed = 3.8).

Table 5
Coke formation for the alkylation and cracking reactions at different reaction conditions.

Catalyst	Temperature (°C)	Time (s)	Conv. (%)	Coke (wt%)	Coke\conv.
Alkylation of toluene with isopropanol					
Y	300	20	56.32	4.45	0.079
Y	250	20	38.93	5.74	0.147
ZSM-5/MCM-48	300	20	23.65	0.40	0.017
ZSM-5/MCM-48	250	20	24.53	0.49	0.020
Catalytic cracking of 1,3,5-triisopropylbenzene					
Y	300	20	53.23	3.89	0.073
ZSM-5/MCM-48	300	20	58.16	0.92	0.016

of 20 s. This value is approximately 11 times more than the coke deposit noticed in the same reaction over ZSM-5/MCM-48 catalyst. The amount of coke deposition over both catalysts was also measured in the catalytic cracking of 1,3,5-triisopropylbenzene at different reaction conditions. The coke formation observed in the catalytic cracking of 1,3,5-triisopropylbenzene over Y-zeolite catalyst is ~3.9 wt% at 300 °C for a reaction time of 20 s. On the other hand, ~0.9 wt% of coke was observed in the cracking reaction over ZSM-5/MCM-48 catalyst, at the same reaction condition. The higher coke formation over Y-zeolite catalyst as compared with ZSM-5/MCM-48 catalyst in both reactions can be attributed to the difference in acidity between both catalysts. Cracking products, with lower molecular weights having lesser diffusion limitations are considered to be the main sources of coke formation [32]. These molecules readily form ion radicals with acid sites of the catalyst, polymerize with other unsaturated hydrocarbons and then dehydrogenate to aggregates of coke [30]. Therefore, due to the high acid sites of Y-zeolite catalyst, coke upon formation, transfers hydrogen to gas phase and/or its adjacent adsorbed components on the high density acid sites of Y-zeolite catalyst.

Overall, the ratio of coke weight percent to percent conversion over both catalysts in the catalytic cracking of 1,3,5-triisopropylbenzene and in the alkylation of toluene with isopropanol is small, ranging from 0.016 to 0.079 at all reaction conditions. Therefore, the catalytic cracking of 1,3,5-TIPB and the alkylation of toluene with isopropanol over both catalysts under study are not accompanied by significant coke formation.

Fig. 14. Effect of 1,3,5-TIPB conversion on benzene (■, ●) and cumene (□, ○) selectivity over Y-zeolite and ZSM-5/MCM-48 catalyst (catalyst/feed = 3.8, reaction temperature 400 °C.

4. Kinetic modeling

In this section, a comprehensive universal kinetic model for alkylation of toluene with isopropanol and the catalytic cracking of 1,3,5-triisopropylbenzene over Y-zeolite catalyst and ZSM-5/MCM-48 catalyst under study was developed. The alkylation of toluene with isopropanol over both catalysts occurs through two main reaction pathways as shown in Scheme 2. To develop a suitable kinetic model representing the overall catalytic cracking of 1,3,5-triisopropylbenzene, we propose the reaction network shown in Scheme 3 and discussed in Section 3.3.

4.1. Model development for alkylation reaction over Y-zeolite and ZSM-5/MCM-48 catalyst

Based on the product distribution observed in the alkylation reaction over both catalysts, a suitable kinetic model representing the overall alkylation reaction can be developed.

It should be noted that the following assumptions were made in deriving the reaction network:

1. Toluene disproportionation follows second order kinetics and a reversible reaction path is assumed for the disproportionation reaction [59,60].
2. Catalyst deactivation is assumed to be a function of time-on-stream (TOS).
3. Isothermal operating conditions can also be assumed given the design of the riser simulator unit and the relatively small amount of reacting species [38].
4. A single effectiveness factor was considered for toluene and cymene.
5. The effectiveness factor η was taken to be unity.

Based on the reaction products noticed in the alkylation of toluene with isopropanol over ZSM-5/MCM-48 catalyst, $k_{x1} \approx 0$, (where $x = z/M$ in the case of ZSM-5/MCM-48 catalyst) in Scheme 1. The disproportionation of toluene in Scheme 2 leading to the formation of benzene and xylenes were neglected due to the inconsistency of these products. The following set of species balances and catalytic reactions were used.

Rate of disappearance of toluene:

$$-\frac{V}{W_c}\frac{dC_T}{dt} = \eta k_{Z/M-2} C_T C_{ISP}\,\exp(-\alpha t) \tag{1}$$

Rate of formation of cymene:

$$\frac{V}{W_c}\frac{dC_{CY}}{dt} = (\eta k_{Z/M-2} C_T C_{ISP} - \eta k_{Z/M-3} C_{CY} C_{ISP})\exp(-\alpha t) \tag{2}$$

Rate of formation of diisopropyltoluene (DIPT):

$$\frac{V}{W_c}\frac{dC_{DIPT}}{dt} = \eta k_{Z/M-3} C_{CY} C_{ISP}\,\exp(-\alpha t) \tag{3}$$

The measurable variables from our chromatographic analysis are the weight fraction of the species, y_x, in the system. By definition

Toluene + Isopropanol $\xrightarrow{k_{X2}}$ Cymene + H$_2$O $\xrightarrow[k_{X3}]{+\text{Isopropanol}}$ DIPT + H$_2$O

$k_{-X1} \big\Updownarrow k_{X1}$

Disproportionation Products

$\big[$ Xylenes + Benzene $\big]$
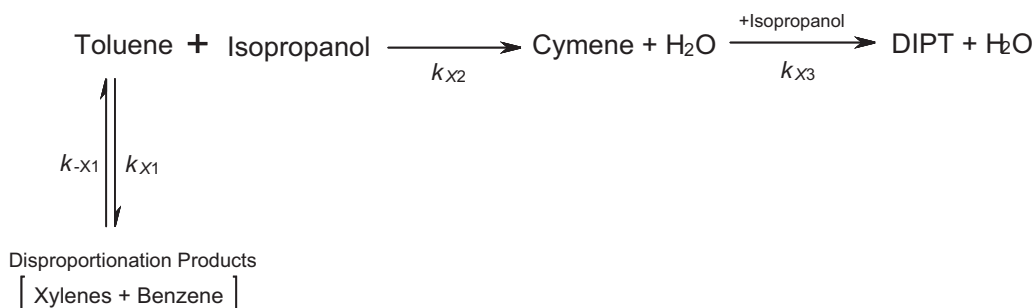
Scheme 2.

the molar concentration, c_x of every species in the system can be related to its mass fraction, y_x by the following relation:

$$c_x = \frac{y_x W_{hc}}{V M W_x} \tag{4}$$

where W_{hc} is the weight of feedstock injected into the reactor, MW_x is the molecular weight of specie x in the system, V is the volume of riser simulator, t = time, α = catalyst decay constant and η = an effectiveness factor to account for the diffusion of toluene, cymenes and diisopropyltoluenes into the pores of the catalyst. Substituting Eq. (4) into Eqs. (1)–(3), we have the following first order differential equations which are in terms of weight fractions of the species:

$$\frac{dy_T}{dt} = -\eta L_1 k_{Z/M-2} y_T y_{ISP} \frac{W_c}{V} \exp(-\alpha t) \tag{5}$$

$$\frac{dy_{CY}}{dt} = [\eta L_2 k_{Z/M-2} y_T y_{ISP} - \eta L_1 k_{Z/M-3} y_{CY} y_{ISP}] \frac{W_c}{V} \exp(-\alpha t) \tag{6}$$

$$\frac{dy_{DIPT}}{dt} = \eta L_3 k_{Z/M-3} y_{CY} y_{ISP} \frac{W_c}{V} \exp(-\alpha t) \tag{7}$$

L_1, L_2 and L_3 are lumped constants given below:

$$L_1 = \frac{W_{hc}}{V M W_{ISP}} \quad L_2 = \frac{MW_{CY} W_{hc}}{V M W_T M W_{ISP}} \quad L_3 = \frac{MW_{DIPT} W_{hc}}{V M W_{CY} M W_{ISP}}$$

Eqs. (5)–(7) contain 5 parameters, $k_{Z/M-2}$, $k_{Z/M-3}$, $E_{Z/M-2}$, $E_{Z/M-3}$, and α, which are to be determined by fitting into experimental data. The temperature dependence of the rate constants was represented with the centered temperature form of the Arrhenius equation, i.e.:

$$k_i = k_{oi} \exp\left[\frac{-E_i}{R}\left(\frac{1}{T} - \frac{1}{T_o}\right)\right] \tag{8}$$

Since the experimental runs were done at 250, 275 and 300 °C, T_0 was calculated to be 275 °C. Where T_0 is an average temperature introduced to reduce parameter interaction [61], k_{oi} is the rate constant for reaction i at T_0, W_c is the weight of catalyst and E_i is the activation energy for reaction i.

In the alkylation of toluene with isopropanol over Y-zeolite catalyst, $k_{x3} \approx 0$, (where $x = Y$ in the case of Y-zeolite catalyst) in Scheme 2. Diisopropyltoluene (DIPT) was not noticed in the reaction product in the alkylation of toluene with isopropanol over Y-zeolite catalyst. Similar assumptions used in the kinetic model development for alkylation of toluene with isopropanol over ZSM-5/MCM-48 catalyst, is also applicable in the alkylation of toluene with isopropanol over Y-zeolite catalyst. The following set of species balances and catalytic reactions can be written.

Rate of disappearance of toluene:

$$\frac{dy_T}{dt} = -\left(2\eta P_1 k_{Y-1} y_T^2 + \eta P_2 k_{Y-2} y_T y_{ISP} - \eta P_3 \frac{k_{Y-1}}{K_{eq}} y_B y_{XY}\right)$$
$$\times \frac{W_c}{V} \exp(-\alpha t) \tag{9}$$

Rate of formation of cymene:

$$\frac{dy_{CY}}{dt} = [\eta P_4 k_{Y-2} y_T y_{ISP}] \frac{W_c}{V} \exp(-\alpha t) \tag{10}$$

Rate of formation of disproportionation products:

$$\frac{dy_{disp}}{dt} = \left(\eta P_5 k_{Y-1} y_T^2 - \eta P_6 \frac{k_{Y-1}}{K_{eq}} y_B y_{XY}\right) \frac{W_c}{V} \exp(-\alpha t) \tag{11}$$

where P_1, P_2, P_3, P_4, P_5 and P_6 are lumped constants given below:

$$P_1 = \frac{W_{hc}}{V M W_T} \quad P_2 = \frac{W_{hc}}{V M W_{ISP}} \quad P_3 = \frac{W_{hc} MW_T}{V M W_B M W_{XY}} \quad P_4 = \frac{W_{hc} MW_{CY}}{V M W_T M W_{ISP}}$$
$$P_5 = \frac{W_{hc} MW_{dispro(avg)}}{V M W_T^2} \quad P_6 = \frac{W_{hc} MW_{dispro(avg)}}{V M W_B M W_{XY}}$$

In order to ensure thermodynamic consistency at equilibrium, the rate constants for toluene to the disproportionation products (benzene + xylene) in the above equations are expressed as follows:

$$k_{-x1} = \frac{k_{x1}}{K_{eq}}$$

where K_{eq} is a temperature-dependent equilibrium constant. The equilibrium constant (K_{eq}) is obtained from a published work [59].

1,3,5-TIPB $\xrightarrow[\text{cracking}]{k_{x1}}$ 1,3-DIPB $\xrightarrow[\text{cracking}]{k_{x2}}$ Cumene $\xrightarrow[\text{cracking}]{k_{x3}}$ Benzene

gases + (above 1,3,5-TIPB product path), gases + Benzene

1,3-DIPB + gases

Cumene $\xdownarrow{k_{x4}}$ disproportionation

DIPBs + Benzene
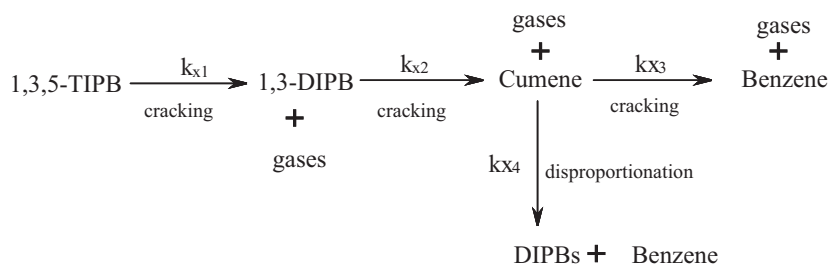
Scheme 3.

4.2. Model development for the catalytic cracking of 1,3,5-triisopropylbenzene over Y-zeolite and ZSM-5/MCM-48 catalyst

To develop a suitable kinetic model representing the catalytic cracking of 1,3,5-triisopropylbenzene, the reaction network shown in Scheme 3 is used. Scheme 3 was adopted based on the various step involved in the catalytic cracking of 1,3,5-triisopropylbenzene over both catalysts under study and as suggested by various researchers [33,34,51].

It should be noted that the following assumptions were made in deriving the reaction network:

1. Cracking reactions follow simple first order kinetics and an irreversible reaction path is assumed for the cracking reaction pathways.
2. The disproportionation of cumene follows second order kinetics and an irreversible reaction path is assumed for the disproportionation reaction.
3. The model assumes catalytic reactions only and neglects thermal conversion.
4. Catalyst deactivation is assumed to be a function of time-on-stream (TOS).

The results of the catalytic cracking of 1,3,5-triisopropylbenzene over ZSM-5/MCM-48 catalyst and Y-zeolite catalyst were modeled using steady state approximations and considering catalyst decay to be a function of time-on-stream. The following set of species balances and catalytic reactions were utilized, where $X = C/CM$ in the case of ZSM-5/MCM-48 catalyst and $X = C/ZY$ in the case of Y-zeolite catalyst.

Rate of 1,3,5-TIPB disappearance:

$$\frac{dy_{\text{TIPB}}}{dt} = -\eta k_{X-1} y_{\text{TIPB}} \frac{W_c}{V} \exp(-\alpha t) \qquad (12)$$

Rate of formation of 1,3-diisopropylbenzene:

$$\frac{dy_{1,3\text{-DIPB}}}{dt} = (\eta S_1 k_{X-1} y_{\text{TIPB}} - \eta k_{X-2} y_{1,3\text{-DIPB}}) \frac{W_c}{V} \exp(-\alpha t) \qquad (13)$$

Rate of formation of cumene (CUM):

$$\frac{dy_{\text{CUM}}}{dt} = (\eta S_2 k_{X-2} y_{1,3\text{-DIPB}} - \eta k_{X-3} y_{\text{CUM}}$$
$$- 2\eta S_3 k_{X-4} y_{\text{CUM}}^2) \frac{W_c}{V} \exp(-\alpha t) \qquad (14)$$

Rate of formation of diisopropylbenzenes (DIPBs):

$$\frac{dy_{\text{DIPB}}}{dt} = \eta S_4 k_{X-4} y_{\text{CUM}}^2 \frac{W_c}{V} \exp(-\alpha t) \qquad (15)$$

Rate of formation of benzene:

$$\frac{dy_{\text{B}}}{dt} = \eta S_5 k_{X-3} y_{\text{CUM}} \frac{W_c}{V} \exp(-\alpha t) \qquad (16)$$

where S_1, S_2, S_3, S_4, and S_5 are lumped constants given below:

$$S_1 = \frac{MW_{1,3\text{-DIPB}}}{MW_{\text{TIPB}}} \quad S_2 = \frac{MW_{\text{CUM}}}{MW_{1,3\text{-DIPB}}} \quad S_3 = \frac{W_{hc}}{VMW_{\text{CUM}}}$$

$$S_4 = \frac{W_{hc} MW_{\text{DIPB}}}{VMW_{\text{CUM}}^2} \quad S_5 = \frac{MW_B}{MW_{\text{CUM}}}$$

In the model development for catalytic cracking of 1,3,5-triisopropylbenzene over Y-zeolite catalyst, $k_{x4} \approx 0$. The disproportionation of cumene (i.e. k_{x4}) was assumed to be equal to zero over Y-zeolite catalyst, due to the inconsistency of the isomers of diisopropylbenzene (mainly para- and ortho-DIPB) and since the maximum amount of para-diisopropylbenzene noticed over Y-zeolite catalyst (∼0.2%) was very small.

Table 6
Estimated kinetic parameters for toluene alkylation over ZSM-5/MCM-48 catalyst values.

Parameters	$k_{Z/M\text{-}2}$	$k_{Z/M\text{-}3}$	α
E_i (kJ/mol)	10.36	5.92	0.05
95% CL	4.48	1.13	0.02
k_{0i}[a] $\times 10^4$ [m³/(kg of catalyst s)]	0.520	0.653	
95% CL $\times 10^4$	0.080	0.158	

$k_{Z/M\text{-}2}$ = rate constant of the primary alkylation reaction over ZSM-5/MCM-48 catalyst; $k_{Z/M\text{-}3}$ = rate constant of the secondary alkylation reaction over ZSM-5/MCM-48 catalyst.

[a] Pre-exponential factor.

Table 7
Correlation matrix for toluene alkylation over ZSM-5/MCM-48 catalyst.

	$k_{Z/M\text{-}2}$	$E_{Z/M\text{-}2}$	α	$k_{Z/M\text{-}3}$	$E_{Z/M\text{-}3}$	α
$k_{Z/M\text{-}2,3}$	1.0000	−0.0885	0.7460	1.0000	−0.0818	0.6337
$E_{Z/M\text{-}2,3}$	−0.0885	1.0000	0.1320	−0.0818	1.0000	0.1216
α	0.7460	0.1320	1.0000	0.6337	0.1216	1.0000

$k_{Z/M\text{-}2,3}$ = rate constant of the primary and secondary alkylation reactions over ZSM-5/MCM-48 catalyst; $E_{Z/M\text{-}2,3}$ = apparent activation energy of the primary and secondary alkylation reactions over ZSM-5/MCM-48 catalyst.

Table 8
Estimated kinetic parameters for toluene alkylation over Y-zeolite catalyst.

Parameters	Values		
	$k_{Y\text{-}1}$	$k_{Y\text{-}2}$	α
E_i (kJ/mol)	22.13	27.73	0.11
95% CL	7.04	14.62	0.05
k_{0i}[a] $\times 10^3$ [m³/(kg of catalyst s)]	0.045	0.034	
95% CL $\times 10^3$	0.006	0.008	

$k_{Y\text{-}1}$ = rate constant of the disproportionation reaction over Y-zeolite catalyst; $k_{Y\text{-}2}$ = rate constant of the primary alkylation reaction over Y-zeolite catalyst.

4.3. Discussion of kinetic modeling results

The kinetic parameters k_{0i}, E_i, and α for the cracking and alkylation reactions were obtained using nonlinear regression (MATLAB package). The values of the model parameters along with their corresponding 95% confidence limits (CLs) are shown in Tables 6, 8–10, while the resulting cross-correlation matrices are also given in Table 7 for ZSM-5/MCM-48 catalyst and Table 11 for Y-zeolite catalyst. Based on the correlation matrices of the regression analysis presented in Table 7 for alkylation of toluene over ZSM-5/MCM-48 catalyst, it shows the very low correlations between $k_{Z/M\text{-}2}$, $k_{Z/M\text{-}3}$ and $E_{Z/M\text{-}2}$, $E_{Z/M\text{-}3}$ and $E_{Z/M\text{-}2}$, $E_{Z/M\text{-}3}$ and α and the moderate correlation between $k_{Z/M\text{-}2}$, $k_{Z/M\text{-}3}$ and α. Similarly, Table 11 reports the very low correlations between $k_{C/ZY\text{-}1}$–$k_{C/ZY\text{-}3}$ and $E_{C/ZY\text{-}1}$–$E_{C/ZY\text{-}3}$ and $E_{C/ZY\text{-}1}$–$E_{C/ZY\text{-}3}$, and α. It can be observed that in the cross-correlation

Table 9
Estimated kinetic parameters for the catalytic cracking of 1,3,5-TIPB over ZSM-5/MCM-48 catalyst.

Parameters	Values				
	$k_{C/CM\text{-}1}$	$k_{C/CM\text{-}2}$	$k_{C/CM\text{-}3}$	$k_{C/CM\text{-}4}$	α
E_i (kJ/mol)	20.09	26.20	43.13	36.06	0.054
95% CL	3.60	9.60	4.61	5.02	0.021
k_{0i}[a] $\times 10^3$ [m³/(kg of catalyst s)]	7.00	13.80	5.84	0.36	
95% CL $\times 10^3$	4.13	3.01	1.47	0.02	

$k_{C/CM\text{-}1}$ = rate constant of the primary cracking reaction over ZSM-5/MCM-48 catalyst; $k_{C/CM\text{-}2}$ = rate constant of the secondary cracking reaction over ZSM-5/MCM-48 catalyst; $k_{C/CM\text{-}3}$ = rate constant of the tertiary cracking reaction over ZSM-5/MCM-48 catalyst; $k_{C/CM\text{-}4}$ = rate constant of the disproportionation reaction over ZSM-5/MCM-48 catalyst.

Table 10
Estimated kinetic parameters for the catalytic cracking of 1,3,5-TIPB over Y-zeolite catalyst.

Parameters	Values			
	$k_{C/ZY-1}$	$k_{C/ZY-2}$	$k_{C/ZY-3}$	α
E_i (kJ/mol)	17.56	13.52	17.29	0.061
95% CL	2.64	7.53	2.16	0.016
$k_{0i}{}^a \times 10^3$ [m³/(kg of catalyst s)]	6.89	17.94	11.34	
95% CL $\times 10^3$	0.66	2.45	2.51	

$k_{C/ZY-1}$ = rate constant of the primary cracking reaction over Y-zeolite catalyst;
$k_{C/ZY-2}$ = rate constant of the secondary cracking reaction over Y-zeolite catalyst;
$k_{C/ZY-3}$ = rate constant of the tertiary cracking reaction over Y-zeolite catalyst.

matrices presented in this study, most of the coefficients remain in the low level with only a few exceptions.

It can be observed from the tabulated results that the apparent activation energy for the disproportionation of toluene over Y-zeolite catalyst was 22.1 ± 7.0. Bhavikatti and Patwardhan [59] reported an apparent energy of activation of ∼60.7 kJ/mol over the Ni/mordenite, while ∼54.3 kJ/mol was reported by Chang et al. [62] for the same reaction over a commercial solid catalyst. The lower energy of activation for the disproportionation of toluene over Y-zeolite catalyst in this present study is expected as compared with the apparent activation energy for the disproportionation of toluene obtained by Bhavikatti and Patwardhan. Y-zeolite catalyst with a diameter of 7.4 Å and the free diameter inside the cages of 12 Å is large enough for the reactants and reaction products as compared to mordenite, in which the cross channels are sufficiently small and with respect to hydrocarbons, the structure is effectively one-dimensional and may be regarded as an array of parallel, noninterconnecting channels [63]. Recently, Odedairo et al. [64] obtained apparent activation energy of 47.0 kJ/mol in toluene transformation over ZSM-5 based catalyst. Considering the pore opening and the pore geometry of ZSM-5 zeolite based catalyst with that of Y-zeolite catalyst used in this study, this result is anticipated. Apparent activation energy ($E_{Z/M-2}$) of 10.4 kJ/mol was obtained for toluene isopropylation over ZSM-5/MCM-48 catalyst. This value is lower than the 27.7 kJ/mol obtained for toluene isopropylation (E_{Y-2}) over the Y-zeolite catalyst. This result indicates that the activation energy required for the formation of cymenes as result of toluene alkylation over Y-zeolite catalyst is higher than the apparent activation energy required for the formation of cymenes over ZSM-5/MCM-48 by magnitudes of 17–18 kJ/mol. The difference in the activation energies may be a clue that the presence of mesopores is crucial for the formation of cymene in toluene alkylation.

Table 9 presents the apparent energies of activation for the catalytic cracking of 1,3,5-triisopropylbenzene over ZSM-5/MCM-48 catalyst. It was noticed that the apparent activation energies in the cracking of 1,3,5-TIPB carried out over the ZSM-5/MCM-48 catalyst follow the order: $E_{C/CM-3\ (tertiary\ cracking)} > E_{C/CM-4\ (disproportionation)} > E_{C/CM-2\ (secondary\ cracking)} > E_{C/CM-1\ (primary\ cracking)}$. From the comparison of the apparent activation energies over ZSM-5/MCM-48 catalyst, we noticed that the reactivity of the alkylbenzenes decreases as the number of propyl group per benzene ring decreases. Similar observation was observed by Akhtar et al.

[65] during the catalytic cracking of 1,3,5-triethylbenzene over a catalyst based on ZSM-5. This is also in agreement with the observation made by Al-Khattaf et al. [66] in their study of catalytic transformation of three methylbenzenes (toluene, m-xylene and 1,2,4-trimethylbenzene) over USY zeolite based catalyst.

The apparent energies of activation for the catalytic cracking of 1,3,5-triisopropylbenzene over Y-zeolite catalyst is presented in Table 10. The apparent energies of activation in the catalytic cracking of 1,3,5-TIPB over Y-zeolite catalyst decreases in the following order: $E_{C/ZY-1\ (primary\ cracking)} > E_{C/ZY-3\ (tertiary\ cracking)} > E_{C/ZY-2\ (secondary\ cracking)}$. The apparent activation energy of 17.6 ± 2.6 kJ/mol was obtained for the formation of 1,3-diisopropylbenzene during the cracking of 1,3,5-TIPB over Y-zeolite catalyst. The secondary cracking reaction of 1,3-DIPB to cumene has lower activation energy (13.5 ± 7.5 kJ/mol) as compared with the primary cracking reaction over Y-zeolite catalyst. It is worth mentioning that 1,3-diisopropylbenzene with a critical diameter of 6.8 Å is able to fit easily into the pores of Y-zeolite, as compared with 1,3,5-triisopropylbenzene with a critical diameter of 9.5 Å. The difference in diffusion of these molecules into the pores of Y-zeolite may account for the difference in apparent activation energies. On the other hand, the alkylbenzene (cumene) became less reactive as compared with 1,3-DIPB, leading to a higher apparent activation energy for the tertiary cracking reaction ($E_{C/ZY-3}$) noticed over Y-zeolite catalyst.
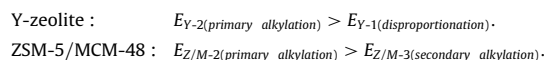
Tukur and Al-Khattaf [67] reported apparent activation energy of 33.4 kJ/mol for the disappearance of 1,3,5-triisopropylbenzene over Y-zeolite catalyst with an acidity of ∼0.03 mmol/g. This value is higher than the apparent activation energy (17.6 kJ/mol) obtained over Y-zeolite catalyst in this study. Since both catalysts are based on the same zeolite, the issue of diffusional limitation is not probably the major contributing factor in explaining the difference in apparent energies of activation noticed over both catalysts. It is a well established fact that the intrinsic activation energy is a function of catalyst acidity. Catalysts of high acidity lead to low intrinsic activation energy. The Y-zeolite catalyst used in this study is much more acidic than the Y-zeolite used by Tukur and Al-Khattaf [67], which is almost likely to lead to a lower intrinsic activation energy over the Y-zeolite catalyst used in this study, as compared with Y-zeolite used by the previous researchers. According to Levenspiel [68] the apparent activation energy is equivalent to half of the summation of the intrinsic activation energy and the diffusion activation energy. Therefore, based on the low intrinsic activation energy over the Y-zeolite catalyst used in this study, a lower apparent energy of activation is expected over this Y-zeolite, as compared with the catalyst based on Y-zeolite used by the previous researchers. From the results of the kinetic parameters presented in Tables 9 and 10, it is observed that the apparent activation energies for the tertiary ($E_{C/ZY-3}$), secondary ($E_{C/ZY-2}$) and primary ($E_{C/ZY-1}$) cracking reactions over Y-zeolite catalyst is lower than the apparent energies of activation noticed over ZSM-5/MCM-48 catalyst in the same reaction. The ease of cracking over Y-zeolite catalyst even though it has smaller pore size as compared with the ZSM-5/MCM-48 catalyst, can be attributed to the higher acidity of Y-zeolite catalyst as compared with ZSM-5/MCM-48 catalyst. To check the validity of the estimated kinetics parameters for

Table 11
Correlation matrix for catalytic cracking of 1,3,5-TIPB over Y-zeolite catalyst.

	$k_{C/ZY-1}$	$E_{C/ZY-1}$	α	$k_{C/ZY-2}$	$E_{C/ZY-2}$	α	$k_{C/ZY-3}$	$E_{C/ZY-3}$	α
$k_{C/ZY-1,2,3}$	1.0000	−0.1019	0.7394	1.0000	−0.1163	0.5307	1.0000	−0.2893	0.5452
$E_{C/ZY-1,2,3}$	−0.1019	1.0000	0.1064	−0.1163	1.0000	0.0397	−0.2893	1.0000	0.0103
α	0.7394	0.1064	1.0000	0.5307	0.0397	1.0000	0.5452	0.0103	1.0000

$k_{C/ZY-1,2,3}$ = rate constant of the primary, secondary and tertiary cracking reactions over Y-zeolite catalyst; $E_{C/ZY-1,2,3}$ = apparent activation energy of the primary, secondary, tertiary cracking reactions over Y-zeolite catalyst.

use at conditions beyond those of the present study, the fitted parameters were substituted into the comprehensive model developed for this scheme and the equations were solved numerically using the fourth-order-Runge-Kutta routine. Graphical comparisons between experimental and model predictions for the time on stream model (TOS) based on the optimized parameters for Scheme 2 is shown in Fig. 8.
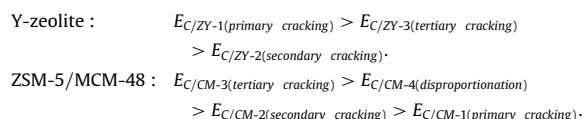
5. Conclusions

The following conclusions can be drawn from the alkylation of toluene with isopropanol and the catalytic cracking of 1,3,5-trisopropylbenzene over Y-zeolite and the ZSM-5/MCM-48 catalyst.

- In the alkylation of toluene with isopropanol, Y-zeolite catalyst and the ZSM-5/MCM-48 catalyst gave significant toluene conversion, but the ZSM-5/MCM-48 catalyst gave much higher cymene selectivity.
- The acidity as well as the pore size of catalysts play a significant role in the catalytic cracking of 1,3,5-triisopropylbenzene.
- In the catalytic cracking of 1,3,5-triisopropylbenzene, precracking of 1,3,5-triisopropylbenzene was observed to be occurring on the surface of the Y-zeolite catalyst.
- The presence of mesopores in ZSM-5/MCM-48 catalyst led to a higher 1,3,5-triisopropylbenzene conversion compared with the catalyst based on Y-zeolite.
- The higher coke formation over Y-zeolite catalyst as compared with ZSM-5/MCM-48 catalyst in both reactions can be attributed to the difference in acidity between both catalysts.
- Kinetic parameters for the alkylation of toluene with isopropanol over both catalysts under study follow the order:

Y-zeolite : $E_{Y\text{-}2(primary\ alkylation)} > E_{Y\text{-}1(disproportionation)}$.

ZSM-5/MCM-48 : $E_{Z/M\text{-}2(primary\ alkylation)} > E_{Z/M\text{-}3(secondary\ alkylation)}$.

- The order of activation energies calculated based on time-on-stream model in the catalytic cracking of 1,3,5-TIPB over both catalysts under study is as follows:

Y-zeolite : $E_{C/ZY\text{-}1(primary\ cracking)} > E_{C/ZY\text{-}3(tertiary\ cracking)}$
$> E_{C/ZY\text{-}2(secondary\ cracking)}$.

ZSM-5/MCM-48 : $E_{C/CM\text{-}3(tertiary\ cracking)} > E_{C/CM\text{-}4(disproportionation)}$
$> E_{C/CM\text{-}2(secondary\ cracking)} > E_{C/CM\text{-}1(primary\ cracking)}$.

References

[1] J.A. Rabo, Appl. Catal. A: Gen. 229 (2002) 7.
[2] L. Huang, W. Guo, P. Deng, Z. Xue, Q. Li, J. Phys. Chem. B 104 (2000) 2817.
[3] M.E. Davies, Nature 417 (2002) 813.
[4] A. Corma, Chem. Rev. 97 (1997) 2373.
[5] C.T. Kresge, M.E. Leonowicz, W.J. Roth, J.C. Vartuli, J.S. Beck, Nature 359 (1992) 710.
[6] L. Wang, A. Wang, X. Li, F. Zhou, Y. Hu, J. Mater. Chem. 20 (2010) 2232.
[7] Y. Xia, R. Mokaya, J. Mater. Chem. 14 (2004) 863.
[8] K.R. Kloetstra, H.W. Zandbergen, J.C. Jansen, H. van Bekkum, Micropor. Mater. 6 (1996) 287.
[9] A. Karlsson, M. Stocker, R. Schmidt, Micropor. Mesopor. Mater. 27 (1999) 181.
[10] D.T. On, S. Kaliaguine, Angew. Chem. Int. Ed. 40 (2001) 3248.
[11] F.S. Xiao, Y. Han, Y. Yu, X. Meng, M. Yang, S. Wu, J. Am. Chem. Soc. 124 (2002) 888.
[12] Y. Liu, W. Zhang, T.J. Pinnavia, Angew. Chem. Int. Ed. 40 (2001) 1255.
[13] Y. Liu, W. Zhang, T.J. Pinnavia, J. Am. Chem. Soc. 122 (2000) 8791.
[14] W. Guo, L. Huang, P. Deng, Z. Xue, Q. Li, Micropor. Mesopor. Mater. 44 (2001) 427.
[15] W. Guo, C. Xiong, L. Huang, Q. Li, J. Mater. Chem. 11 (2001) 1886.
[16] Z. Zhang, Y. Han, L. Zhu, R. Wang, Y. Yu, S. Qiu, D. Zhao, F.S. Xiao, Angew. Chem. Int. Ed. 40 (2001) 1258.
[17] Z. Zhang, Y. Han, F.S. Xiao, S. Qiu, L. Zhu, R. Wang, Y. Yu, Z. Zhang, B. Zou, Y. Wang, H. Sun, D. Zhao, Y. Wen, J. Am. Chem. Soc. 123 (2001) 5014.
[18] P. Prokesova, S. Mintova, J. Cejka, T. Bein, Micropor. Mesopor. Mater. 64 (2003) 165.
[19] K. Ito, Hydrocarbon process. 52 (1973) 82.
[20] K.S.N. Reddy, B.S. Rao, V.P. Shiralkar, Appl. Catal. A: Gen. 121 (1995) 191.
[21] D. Fraenkel, M. Levy, J. Catal. 118 (1989) 10.
[22] B. Wichterlova, J. Cejka, Micropor. Mater. 6 (1996) 405.
[23] B. Wichterlova, J. Cejka, J. Catal. 146 (1994) 523.
[24] J. Cejka, G.A. Kapustin, B. Wichterlova, Appl. Catal. A 108 (1994) 187.
[25] T. Odedairo, S. Al-Khattaf, Chem. Eng. J. (2011), doi:10.1016/j.cej.2010.12.043.
[26] J.M. Valtierra, M.A. Sanchez, J.A. Montoya, J. Navarrete, J.A. de los Reyes, Appl. Catal. A: Gen. 158 (1997) L1.
[27] R. Savidha, A. Pandurangan, Appl. Catal. A 276 (2004) 39.
[28] G.D. Yadav, S.A. Purandare, Micropor. Mesopor. Mater. 103 (2007) 363.
[29] R. Sadeghbeigi, Fluid Catalytic Cracking Handbook: Design, Operation and Troubleshooting of FCC Facilities, Gulf Publishing Company, Austin, TX, 2000.
[30] N. Hosseinpour, A.A. Khodadadi, Y. Mortazavi, A. Bazyari, Appl. Catal. A 353 (2009) 271.
[31] N. Hosseinpour, Y. Mortazavi, A. Bazyari, A.A. Khodadadi, Fuel Process. Technol. 90 (2009) 171.
[32] A. Bazyari, A.A. Khodadadi, N. Hosseinpour, Y. Mortazavi, Fuel Process. Technol. 90 (2009) 1226.
[33] P. Morales-Pacheco, J.M. Dominguez, L. Bucio, F. Alvarez, U. Sedran, M. Falco, Catal. Today (2010), doi:10.1016/j.cattod.2010.07.005.
[34] S. Al-Khattaf, J.A. Atias, K. Jarosch, H. de Lasa, Chem. Eng. Sci. 57 (2002) 4909.
[35] J. Qi, T. Zhao, X. Xu, F. Li, G. Sun, C. Miao, H. Wang, Catal. Today 10 (2009) 1523.
[36] Y. Sun, L. Zhu, H. Lu, R. Wang, S. Lin, D. Jiang, F.S. Xiao, Appl. Catal. A 237 (2002) 21.
[37] E.P. Barrett, L.G. Joyner, P.P. Halenda, J. Am. Chem. Soc. 73 (1951) 373.
[38] H.I. de Lasa, Riser simulator for catalytic cracking studies, U.S. Patent 5,102 (1991) 628.
[39] T. Odedairo, S. Al-Khattaf, Chem. Eng. J. 157 (2010) 204.
[40] T. Odedairo, S. Al-Khattaf, Ind. Eng. Chem. Res. 49 (2010) 1642.
[41] Y. Xia, R. Mokaya, J. Mater. Chem. 13 (2003) 657.
[42] Y. Xia, R. Mokaya, J. Mater. Chem. 14 (2004) 3427.
[43] J.S. Beck, J.C. Vartulli, W.J. Roth, M.E. Leonowicz, C.T. Kresge, K.D. Schmitt, C.T.W. Chu, D.H. Olson, E.W. Sheppard, S.B. McCullen, J.B. Higgins, J.L. Schlenker, J. Am. Chem. Soc. 114 (1992) 10834.
[44] Y. Li, J. Shi, Z. Hua, H. Chen, M. Ruan, D. Yan, Nano Lett. 3 (2003) 609.
[45] G.D. Yadav, S.S. Salgaonkar, Micropor. Mesopor. Mater. 80 (2005) 129.
[46] G.D. Yadav, S.S. Salgaonkar, Ind. Eng. Chem. Res. 44 (2005) 1706.
[47] A. Corma, B.W. Wojciechowski, Catal. Rev. Sci. Eng. 24 (1982) 1.
[48] S. Al-Khattaf, H. de Lasa, Appl. Catal. A: Gen. 226 (2002) 139.
[49] T.C. Tsai, S.B. Liu, I. Wang, Appl. Catal. A: Gen. 181 (1999) 355.
[50] N. Al-Baghli, S. Al-Khattaf, Stud. Surf. Sci. Catal. 158 (2005) 1661.
[51] A. Mahgoub, S. Al-Khattaf, Energy Fuels 19 (2005) 329.
[52] L. Zhu, S. Xiao, Z. Zhang, Y. Sun, Y. Han, S. Qiu, Catal. Today 68 (2001) 209.
[53] H. Koch, W. Reschetilowski, Mesopor. Mater. 25 (1998) 127.
[54] N. Katada, Y. Kageyamaa, K. Takahara, T. Kanai, H.A. Beguma, M. Niwa, J. Mol. Catal. A: Chem. 211 (2004) 119.
[55] Q. Tan, X. Bao, T. Song, Y. Fan, G. Shi, B.S.C. Liu, X. Gao, J. Catal. 251 (2007) 69.
[56] B.A. Watson, M.T. Klein, R.H. Harding, Appl. Catal. A: Gen. 160 (1997) 13.
[57] J. Cejka, J. Kotria, A. Krejci, Appl. Catal. A 277 (2004) 191.
[58] S. Al-Khattaf, N.M. Tukur, S. Rabiu, Ind. Eng. Chem. Res. 48 (2009) 2843.
[59] S.S. Bhavikatti, S.R. Patwardhan, Ind. Eng. Chem. Prod. Res. Dev. 20 (1981) 106.
[60] X.U. Ouguan, S.U. Hongye, J.I. Jianbing, J.I.N. Xiaoming, C.H.U. Jian, Chin. J. Chem. Eng. 15 (2007) 326.
[61] A.K. Agarwal, M.L. Brisk, Ind. Eng. Chem. Process Des. Dev. 24 (1985) 203.
[62] J.R. Chang, F.C. Sheu, Y.M. Cheng, J.C. Wu, Appl. Catal. 33 (1987) 39.
[63] C.N. Satterfield, Heterogeneous Catalysis in Industrial Practice, 2nd ed., Krieger Publishing Company, Malabar, FL, 1996.
[64] T. Odedairo, R.J. Balasamy, S. Al-Khattaf, Ind. Eng. Chem. Res. 50 (2011) 3169.
[65] M.N. Akhtar, N.M. Tukur, N. Al-Yassir, S. Al-Khattaf, J. Cejka, Chem. Eng. J. 163 (2010) 98.
[66] S. Al-Khattaf, N.M. Tukur, A. Al-Amer, U.A. Al-Mubaiyedh, Appl. Catal. A: Gen. 305 (2006) 21.
[67] N.M. Tukur, S. Al-Khattaf, Chem. Eng. Process. 44 (2005) 1257.
[68] O. Levenspiel, Chemical Reaction Engineering, 3rd ed., John Wiley & Sons, New York, 1999.